

# Compensation of beam-beam effects in the Tevatron with wires

B. Erdelyi\*and T. Sen  
Fermilab, MS 220  
PO Box 500  
Batavia, IL 60510

## Abstract

We explore the possibility of compensating long-range beam-beam interactions in the Tevatron by current carrying wires. At injection we attempt to compensate all interactions with four wires placed around the ring in four warm straight sections. At collision energy the compensation of the four long-range interactions nearest to B0 and D0 is studied. We study in some detail strategies where the wires are placed at the same locations as the beam-beam interactions (local compensation) as well as strategies with the wires placed at different longitudinal locations (non-local compensation). Possible strategies with multiple wires at the same location are briefly discussed.

## Contents

<b>1</b>	<b>Introduction</b>	<b>3</b>
<b>2</b>	<b>Local compensation</b>	<b>5</b>
2.1	Beam-beam kicks . . . . .	5
2.2	Principle of the correction . . . . .	6
2.3	Round wires . . . . .	6
2.3.1	Local compensation of round beams . . . . .	7
2.3.2	Local Correction of One Elliptic Beam-Beam Interaction . . . . .	10
2.4	Elliptic cylindrical wires . . . . .	16
2.4.1	Approximation of the elliptical wire kicks by round wire kicks . . . . .	20
<b>3</b>	<b>Non-local compensation</b>	<b>21</b>
3.1	Analytical Results . . . . .	21
3.1.1	One beam-beam kick . . . . .	22
3.1.2	Two beam-beam interactions compensated by a single wire . . . . .	23
3.1.3	Several beam-beam interactions compensated by a single wire . . . . .	24
3.2	Simulation Results . . . . .	25
<b>4</b>	<b>Studies at Injection Energy</b>	<b>30</b>
<b>5</b>	<b>Multiple wires at a single location</b>	<b>32</b>
<b>6</b>	<b>Summary</b>	<b>34</b>
<b>A</b>	<b>Appendix: Optics changes due to beam-beam interactions</b>	<b>35</b>
<b>B</b>	<b>Appendix: Optics changes due to the field of a wire</b>	<b>37</b>

\*Now at Northern Illinois University, Dekalb, IL 60115

<b>C Appendix: Average beam-beam kick</b>	<b>40</b>
C.1 Special case of round beams . . . . .	41

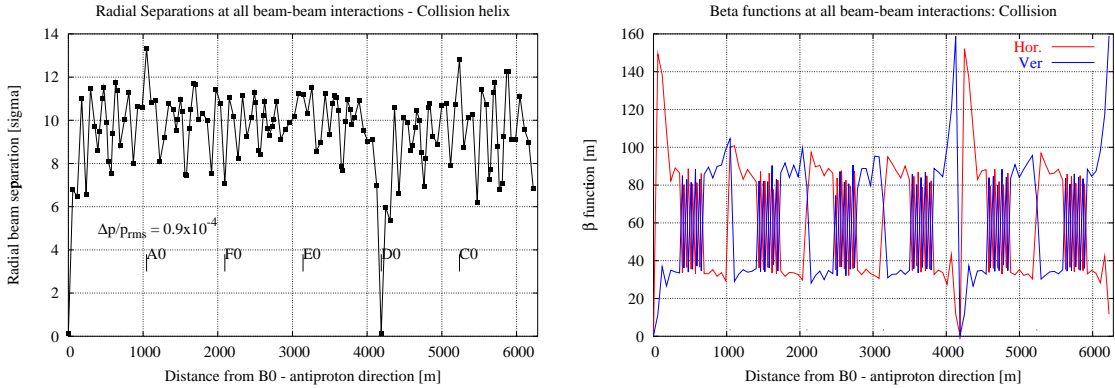


Figure 1: Beam separations (left) and beta functions (right) at all the beam-beam interactions at 980 GeV. The parasitics on either side of B0 and D0 occur at small separations and large beta functions.

## 1 Introduction

Long-range beam-beam interactions are known to cause anti-proton beam loss at several stages of the Tevatron operational cycle. The idea of compensating their effects by current carrying wires was originally proposed for the LHC [1]. Early theoretical results for the LHC suggested that wires could be useful in increasing the dynamic aperture [2]. Recently machine studies performed at the CERN SPS have examined the effects of a single wire on a single beam [3]. More studies in the SPS with several wires are scheduled in 2004.

The optics and dynamics of the long-range interactions are significantly more complex in the Tevatron than in the LHC. In the LHC all long-range interactions occur within approximately 60 m on either side of the main interaction points (IPs) and these long-range interactions are all roughly at the same betatron phase. In the Tevatron the long-range interactions occur all around the ring and at very different phases. Nevertheless the idea of compensating a few well selected interactions with wires is a promising one. This report focuses mainly on our studies of wire compensation at top energy. Wire compensation at injection energy was studied earlier and reviewed in October 2003 [4]. We also point out that a brief simulation study of wire compensation in the Tevatron was reported by F. Zimmermann using his code [5].

At 980 GeV it is relatively easy to identify the parasitic interactions that are most likely to be dominant. Figure 1 shows the radial beam separation (in units of the rms beam size) and the beta functions at all the locations of the beam-beam interactions. The parasitics on either side of B0 and D0 occur at small separations and the beta functions are large.

Figure 2 shows the small amplitude tune shifts from each individual parasitic. The nearest parasitics around B0 and D0 contribute the largest tune shifts among all the parasitics. These four parasitics are therefore most likely to be the most dominant ones.

Figure 3 shows the diffusion coefficients calculated with the code **BBSIM** [6] at a  $5\sigma$  amplitude from individual beam-beam interactions. While the 4 nearest parasitics are important, there are several others that lead to diffusion coefficients of similar magnitude. The relative importance of the parasitics also changes at other amplitudes. This diffusion calculation complicates the simple interpretation suggested by the tune-shift calculation and suggests that several interactions may have to be compensated.

On the other hand we will only be able to compensate a limited number of parasitics. We therefore examine the diffusion when we exclude the four nearest parasitics. Excluding them is equivalent to a perfect compensation of these interactions. Figure 4 shows the diffusion coefficients at several transverse amplitudes. The diffusion coefficients at amplitudes up to  $5\sigma$  are noticeably smaller when these four parasitics are missing. In this report we will study mainly the compensation of these parasitics at 980 GeV.

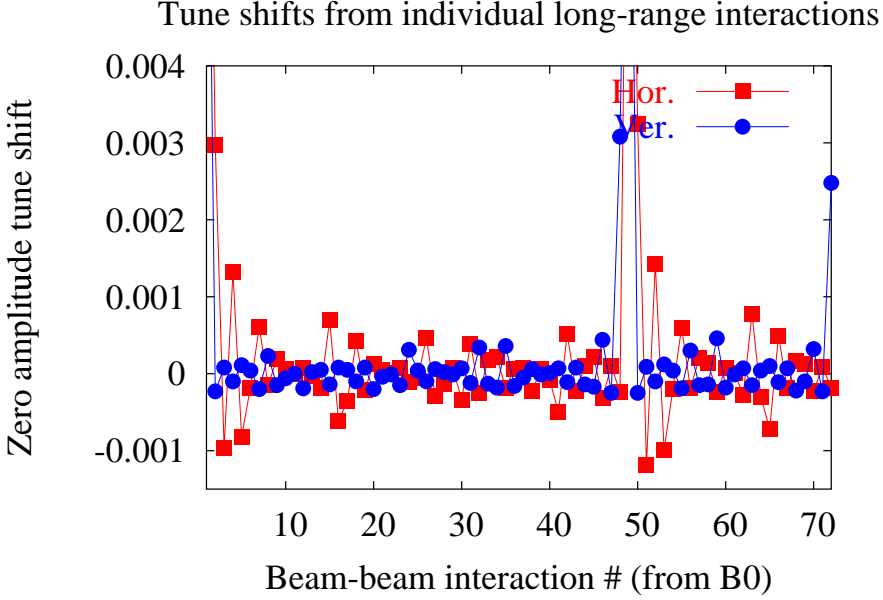


Figure 2: Tune shifts at zero amplitude from individual long-range interactions for anti-proton bunch 6 at low beta (980 GeV). The tune shifts from the collision points at B0 and D0 are off scale. The 4 parasitics, 2 around B0 and 2 around D0, contribute the largest tune shifts among all the parasitics.

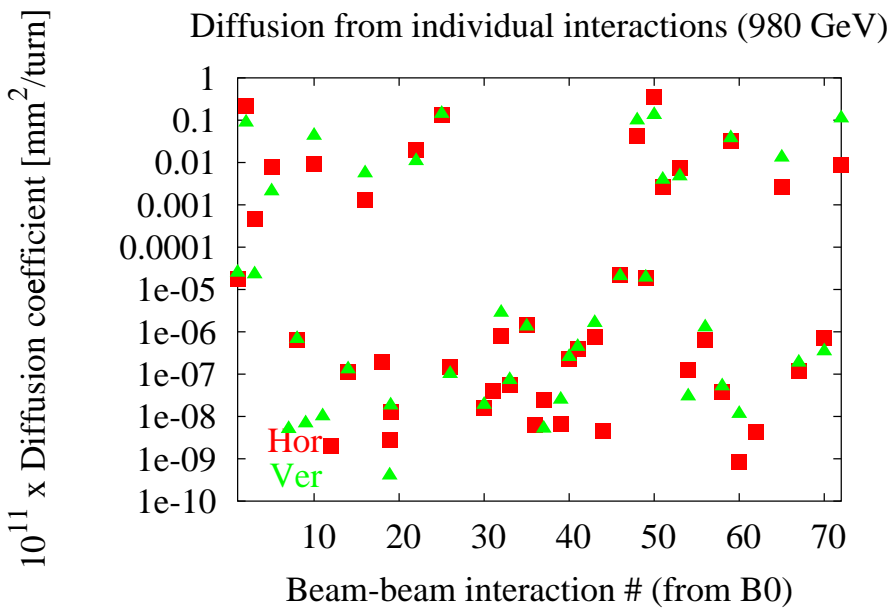


Figure 3: Diffusion coefficients at a  $5\sigma$  transverse amplitude due to individual beam-beam interactions. B0 is interaction number 1, D0 is number 49 so the parasitics around B0 are numbered (2, 72) and around D0 are numbered (48,50) respectively. While these 4 parasitics do cause large diffusion, several other interactions are also of similar magnitude. The proton bunch intensity was set to 10 times the nominal intensity in order to increase the diffusion.

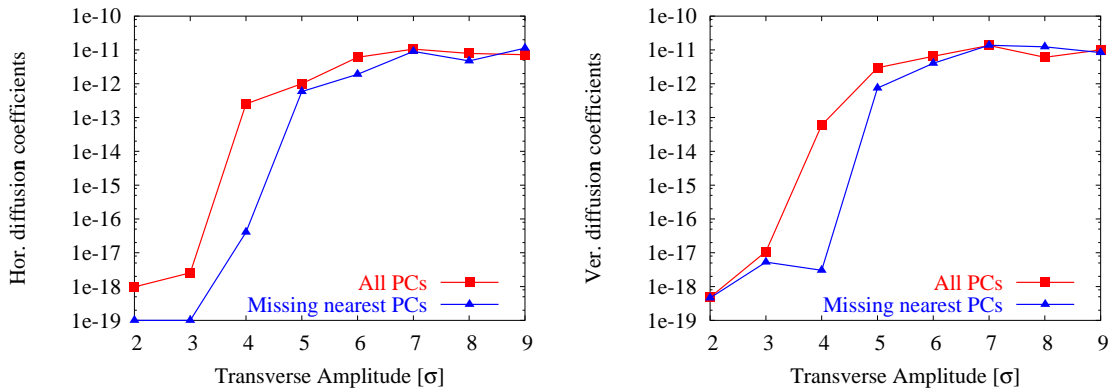


Figure 4: Diffusion coefficients with and without the 4 nearest parasitics. Left: Horizontal coefficients, Right: Vertical coefficients

## 2 Local compensation

We present the principles and theory of the compensation in this section. After a review of the relevant beam-beam effects, the kicks due to round and cylindrical elliptic wires are presented. Comparisons with the beam-beam induced kicks will be shown, as well as ideas about correction of several beam-beam kicks by wires.

### 2.1 Beam-beam kicks

For a general, elliptic Gaussian cylindrical strong beam the kicks felt by a test particle in the weak beam are given by the well-known Basetti-Erskine formulae. Assuming that the horizontal beam size is larger than the vertical ( $\sigma_x > \sigma_y$ ) and  $x, y > 0$ :

$$\Delta x' = \frac{N_b r_p}{\gamma_p} \sqrt{\frac{2\pi}{\sigma_x^2 - \sigma_y^2}} \operatorname{Im} F(x, y), \quad \Delta y' = \frac{N_b r_p}{\gamma_p} \sqrt{\frac{2\pi}{\sigma_x^2 - \sigma_y^2}} \operatorname{Re} F(x, y) \quad (1)$$

where

$$F(x, y) = W\left(\frac{x + iy}{\sqrt{2(\sigma_x^2 - \sigma_y^2)}}\right) - \exp\left(-\frac{x^2}{2\sigma_x^2} - \frac{y^2}{2\sigma_y^2}\right) W\left(\frac{\frac{\sigma_y}{\sigma_x}x + i\frac{\sigma_x}{\sigma_y}y}{\sqrt{2(\sigma_x^2 - \sigma_y^2)}}\right),$$

and  $N_b$  is the strong beam intensity,  $r_p$  is the classical proton radius,  $\gamma_p$  is the relativistic factor, and  $W$  is the complex error function.  $(x, y)$  are the coordinates of the test particle relative to the centroid of the strong beam. If  $\sigma_y > \sigma_x$  the expressions for the kicks can be obtained by interchanging  $x$  and  $y$ . For other signs of  $x$  and  $y$  the kicks are obtained noticing that  $\Delta x'$  is odd in  $x$  and even in  $y$ , and vice versa for  $\Delta y'$ .

If the strong beam is close to being round ( $\sigma_x \approx \sigma_y$ ), the complex error functions argument modulus tends to infinity, so an asymptotic expansion and retention of the first expansion term should give a fairly accurate result. In this case,

$$W(z) \xrightarrow{\|z\| \rightarrow \infty} e^{-z^2} + \frac{i}{\sqrt{\pi}z} \left(1 + \frac{1}{2z^2} + \frac{3}{4z^4} + \dots\right),$$

and if the term in parenthesis is approximated by 1 the kicks become

$$\begin{aligned} \Delta x' &= \frac{2N_b r_p}{\gamma_p} x \left[ \frac{1}{x^2 + y^2} - \sigma_y^2 \frac{\sigma_x \sigma_y}{\sigma_y^4 x^2 + \sigma_x^4 y^2} \exp\left(-\frac{x^2}{2\sigma_x^2} - \frac{y^2}{2\sigma_y^2}\right) \right], \\ \Delta y' &= \frac{2N_b r_p}{\gamma_p} y \left[ \frac{1}{x^2 + y^2} - \sigma_y^2 \frac{\sigma_x \sigma_y}{\sigma_y^4 x^2 + \sigma_x^4 y^2} \exp\left(-\frac{x^2}{2\sigma_x^2} - \frac{y^2}{2\sigma_y^2}\right) \right]. \end{aligned} \quad (2)$$

In particular, if the beam is exactly round ( $\sigma = \sigma_x = \sigma_y$ ), the term in parenthesis becomes exactly 1, and hence the kicks due a round beam are

$$\Delta x' = \frac{2N_b r_p}{\gamma_p} \frac{x}{x^2 + y^2} \left[ 1 - \exp \left( -\frac{x^2 + y^2}{2\sigma^2} \right) \right], \quad \Delta y' = \frac{2N_b r_p}{\gamma_p} \frac{y}{x^2 + y^2} \left[ 1 - \exp \left( -\frac{x^2 + y^2}{2\sigma^2} \right) \right] \quad (3)$$

These equations show that if one finds a correction scheme for round beams, the same correction will work for beams not too far from round, that is, the correction would be robust against small perturbation in the optics or other parameters. Since the asymptotic expansion is also valid for large distances, they show that the field lines of the elliptic Gaussian beam become circles.

## 2.2 Principle of the correction

As one can see from (3), the force field lines are circular for a round beam, corresponding to a radial electric field that is inversely proportional with the distance from the beam centroid. If one could create also an azimuthal magnetic field with the same dependence on the distance, by appropriately choosing the parameters one could cancel exactly the beam-beam kicks by the kicks induced by the magnetic field.

It is well-known that an infinitely long straight current carrying wire creates just the field that is needed, and by appropriate placement and current cancellation can be achieved. However, it is also clear that in the region where the exponential part of the beam-beam kicks play an important role, the compensation will fail. Therefore, we can hope that we can correct parasitic beam-beam kicks for amplitudes of test particles which lie outside the core of the strong beam, since the exponential part becomes insignificant at about a distance of  $3\sigma$  from the strong beam centroid.

If the beams are very elliptical and they are not very far apart, then the above arguments suggest that it may not be possible to compensate the beam-beam effects by round wires. But in the same way that the level lines of a round Gaussian charge distribution are circles, and the kicks can be corrected by round wires, one can hope that the elliptic Gaussian beam kicks could be compensated by elliptic cylindrical wires, since the level lines of the elliptical Gaussian distribution are ellipses. We will show that indeed this is the case. Moreover, the best achievable correction of an elliptic Gaussian kick by the kick of a round wire will be presented.

## 2.3 Round wires

The field lines of an infinitely long straight wire are concentric circles with the wires axis, and has the magnitude of

$$|\vec{B}| = \frac{\mu_0 I_W}{2\pi r}, \quad (4)$$

where  $r$  is the distance from the wire. A more accurate calculation, for the kicks due to a finite length wire, embedded in the middle of a drift of length  $L$  is given by

$$\Delta x' = - \int_{-L/2}^{L/2} \frac{B_y}{(B\rho)} dz, \quad \Delta y' = \int_{-L/2}^{L/2} \frac{B_x}{(B\rho)} dz. \quad (5)$$

The magnetic field can be computed using the Biot-Savart law. Assume that in an arbitrary coordinate system  $(x, y, z)$  we have a wire of length  $l$ , such that the start of the wire is at a distance  $\vec{r}_P$  from a point  $P$  where we want to compute the field. If the length of the wire is parameterized by  $\lambda$  such that  $\vec{l}(\lambda) = \lambda \vec{l}$  with  $\lambda \in [0, 1]$ , the field, integrated over  $L$ , is given by

$$\langle \vec{B}_P \rangle = 10^{-7} I_W \int_{-L/2}^{L/2} dz \int_0^1 d\lambda \frac{\vec{l} \times \vec{r}_P}{|\vec{r}_P - \lambda \vec{l}|^3}, \quad (6)$$

where  $I_W$  is the current.

The integrals can be done analytically. However, they simplify if the coordinate system is assumed parallel to the wire, that is, if  $\vec{l} = (l_x, l_y, l_z)$ , the coordinate system is oriented such that  $l_x = l_y = 0$ . In

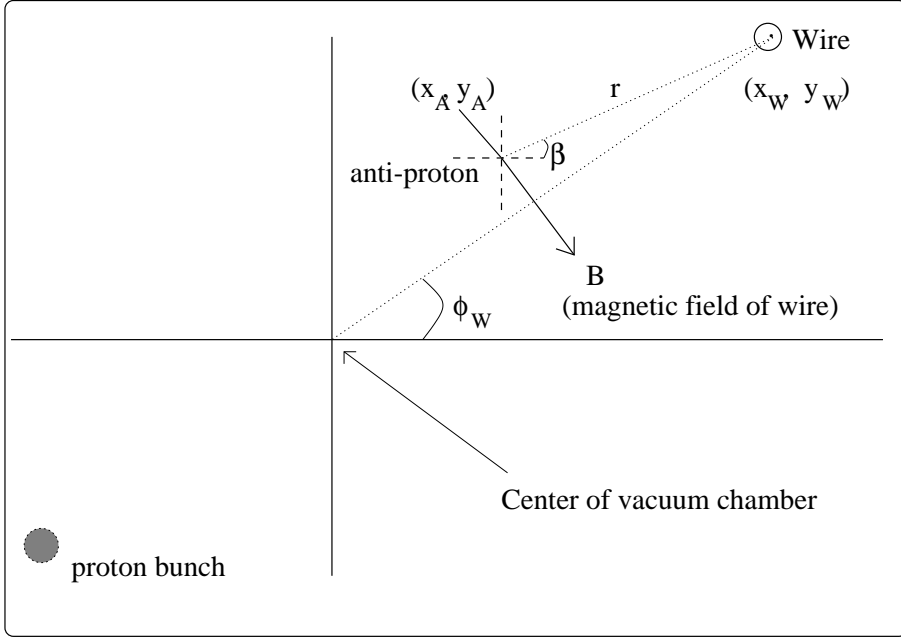


Figure 5: Coordinates of the wire, test anti-proton and proton bunch. Current in the wire is directed out of the plane of the paper.

this case the result is given by

$$\langle \vec{B}_P \rangle = 10^{-7} I \frac{u - v}{x^2 + y^2} \begin{pmatrix} x \\ y \\ 0 \end{pmatrix}, \quad (7)$$

where  $u = \sqrt{\left(\frac{L}{2} + l\right)^2 + x^2 + y^2}$  and  $v = \sqrt{\left(\frac{L}{2} - l\right)^2 + x^2 + y^2}$ . Here  $x$  and  $y$  are regarded as the sums of the wire distance from the weak beam's centroid and the particle's betatron amplitude. In case the wire is tilted with respect to the coordinate system, first the tilt of the coordinate system is performed. The case of an infinite wire can be obtained in the limit  $L \rightarrow \infty$ , in which case  $u - v \rightarrow 2l$ , and (4) is recovered.

### 2.3.1 Local compensation of round beams

We consider the opposing proton beam to be round in this section. The origin of coordinates is chosen to be at the center of the vacuum chamber. If the coordinates of the proton centroid are  $(x_{P0}, y_{P0})$  and the coordinates of the test anti-proton particle are  $(x_A, y_A)$ , the beam-beam kicks experienced by the anti-proton are

$$\Delta x'_{BB} = \frac{2N_p r_p}{\gamma_p} \frac{x_A - x_{P0}}{[(x_A - x_{P0})^2 + (y_A - y_{P0})^2]} \left\{ 1 - \exp[-\frac{1}{2\sigma^2} [x_A - (x_{P0})^2 + (y_A - y_{P0})^2]] \right\} \quad (8)$$

$$\Delta y'_{BB} = -\frac{2N_p r_p}{\gamma_p} \frac{y_A - y_{P0}}{[(x_A - x_{P0})^2 + (y_A - y_{P0})^2]} \left\{ 1 - \exp[-\frac{1}{2\sigma^2} [(x_A - x_{P0})^2 + (y_A - y_{P0})^2]] \right\} \quad (9)$$

If the two beams are sufficiently far away that the argument of the exponential is  $\gg 1$ , then the exponential term has a negligible contribution and only the first term in  $\{ \}$  need be kept.

Now consider the field and forces due to a wire on the test anti-proton. From Figure 5 it follows that the components of the field are

$$B_x = |B| \sin \beta = \frac{\mu_0}{2\pi} \frac{y_W - y_A}{r^2} I_W, \quad B_y = -|B| \cos \beta = -\frac{\mu_0}{2\pi} \frac{x_W - x_A}{r^2} I_W \quad (10)$$

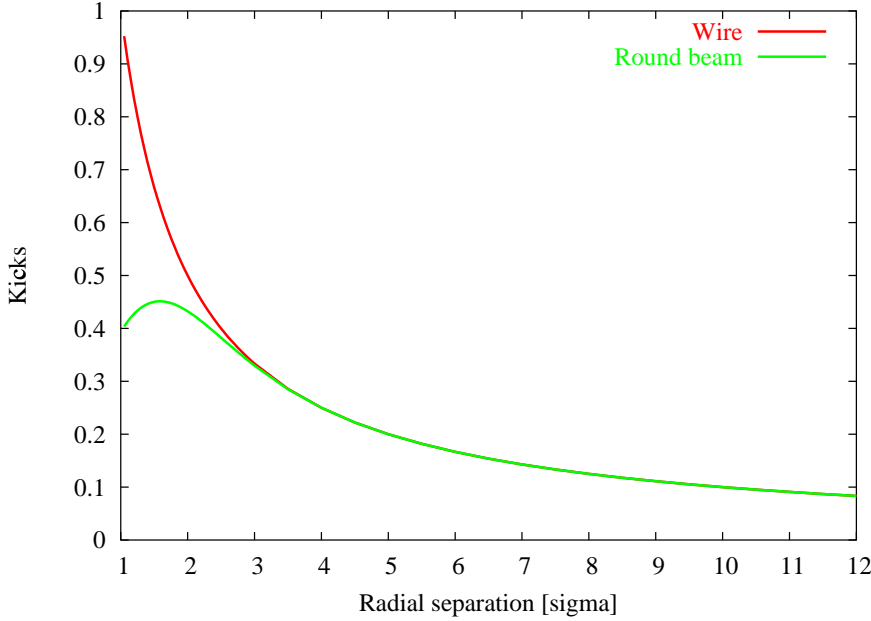


Figure 6: Kicks from a round beam compared to the kick of a round wire as a function of distance. At distances larger than  $3\sigma$ , the kicks agree to better than 1%.

Here

$$r^2 = (x_W - x_A)^2 + (y_W - y_A)^2$$

Assuming that the force due to the wire can be lumped in the middle of the wire and considered as that due to an impulsive force, the change in slopes of the anti-proton are

$$\Delta x'_W = -\frac{B_y L}{(B\rho)} = \frac{\mu_0 I_W L}{2\pi(B\rho)} \frac{x_W - x_A}{(x_W - x_A)^2 + (y_W - y_A)^2} \quad (11)$$

$$\Delta y'_W = \frac{B_x L}{(B\rho)} = \frac{\mu_0 I_W L}{2\pi(B\rho)} \frac{y_W - y_A}{(x_W - x_A)^2 + (y_W - y_A)^2} \quad (12)$$

Figure 6 compares the kicks from a round beam with that of a round wire. At separations larger than  $3\sigma$ , the field profiles match very closely. At large distances we can be justified in dropping the exponential part of the beam-beam kick. Cancelling the beam-beam kicks with those of a round wire requires  $\Delta x_{BB} + \Delta x'_W = 0 = \Delta y_{BB} + \Delta y'_W$  or

$$x_W = x_{P0}, \quad y_W = y_{P0}, \quad (13)$$

$$\frac{\mu_0 I_W L}{2\pi(B\rho)} = \frac{2N_p r_p}{\gamma_p} \Rightarrow I_W L = ecN_p \quad (14)$$

This cancellation is achieved for any test particle amplitude  $(x_A, y_A)$  provided that the test particle is sufficiently far ( $> 3\sigma$ ) from the strong beam. This particular solution requires that the wire be placed next to the proton beam. At the design proton intensity of  $2.7 \times 10^{11}$  particles per bunch, the integrated current required is 13 Amp-m.

We now turn to simulations of the compensation of a round-beam by a round wire. The aspect ratio of the proton beam at the location of the interactions vary in the region [0.25, 4]. See Fig. 7 for the case of anti-proton bunch #6. Among the 70 parasitics one (#22 in the figure) is the closest to being round, so we used it as a test case to check the theory and the code. As the separation at this parasitic is around  $6.6\sigma$ , we expect that compensation is achieved at least for anti-proton amplitudes of up to  $3\sigma$ . For larger amplitudes we expect that the exponential part of the beam-beam kick becomes important, and the correction will be spoiled. Indeed, this is what we observed. Fig. 8 shows that the diffusion

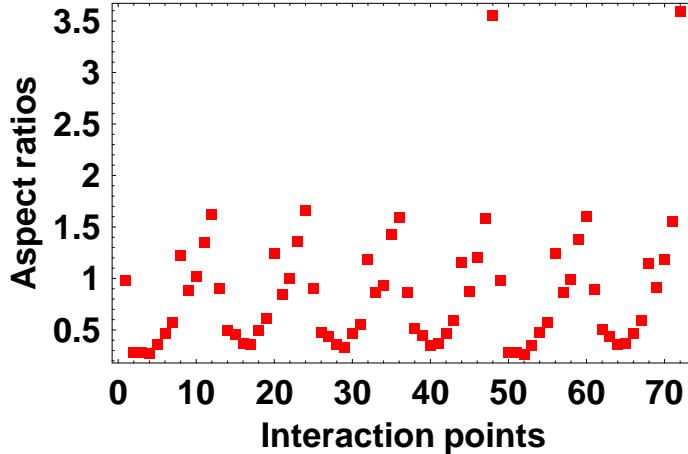


Figure 7: The proton beam aspect ratios at the location of the beam-beam interactions at collision. #22 is closest to being round, #1 is B0, and #49 is D0.

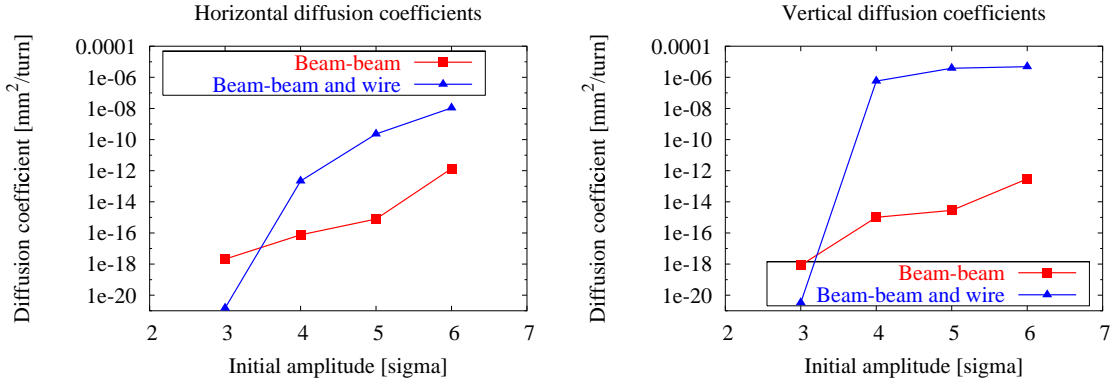


Figure 8: Diffusion coefficients for the local correction of the round parasitic #22 where the beam separation is about  $6.6\sigma$ . The compensating wire lowers the diffusion coefficients of anti-protons only at the  $3\sigma$  amplitude but not at higher amplitudes where the anti-protons are much closer to the strong proton bunch. Left panel: horizontal, Right panel: vertical coefficients

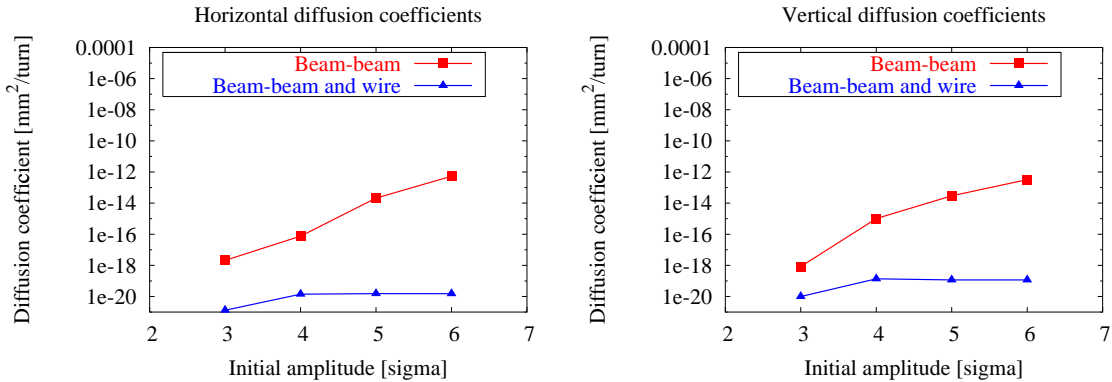


Figure 9: Diffusion coefficients for the local correction of the round parasitic #22, when the separation is approximately  $10\sigma$ . In contrast to Figure 8, the diffusion coefficients with the compensating wire are now smaller at amplitudes up to  $6\sigma$ . Left panel: horizontal, Right panel: vertical coefficients

coefficient is reduced to practically zero for a starting amplitude of  $3\sigma$  but the diffusion increases for particles at larger amplitudes. Another check of the importance of the exponential part is obtained by artificially increasing the separation by 50%. As seen in Fig. 9, indeed now all diffusion coefficients for amplitudes up to  $6\sigma$  are practically vanishing. Smaller diffusion coefficients also reduced the emittance growth in the simulations. Therefore, the simulations confirm what we expected from theory.

While this simulation demonstrates the compensation principle at work, it is not very practical for the Tevatron for at least two reasons: (i) beams are not round at most locations and (ii) wires cannot be placed at every location of a beam-beam interaction. We address the first of these issues in the next section.

### 2.3.2 Local Correction of One Elliptic Beam-Beam Interaction

The most direct compensation strategy is to correct the field of the strong beam by a wire. This strategy worked, i.e. reduced the diffusion, in the case of a round beam compensated by a round wire. We examine this possibility now for the case of an elliptical beam. The difference between the kicks due to a very elliptical beam and a round wire can be substantial. Figure 10 shows the relative % error between these kicks for a beam with an aspect ratio of 0.25. The elliptical beam-beam kick is significantly smaller than the  $1/r$  kick in the horizontal plane up to separations of  $10\sigma$ . The error drops to the 1% level only at separations greater than  $20\sigma$ . In the vertical plane the beam-beam kick is significantly smaller up to separations of  $3.5\sigma$ , is larger for larger separations and approximates the  $1/r$  kick at the 1% level only for separations greater than  $20\sigma$ . Figure 11 shows the minimum separation required for the average kick due to the field of a wire to match the average kick due to the field of an elliptical beam to within 1%. The aspect ratios in the Tevatron range between 0.25 - 3.5 with the extremes occurring at low beta at the nearest parasitics around B0 and D0. It is clear that the optimum transverse separation of the wire depends strongly on the aspect ratio of the strong beam at the beam-beam interaction that needs to be compensated.

Consider the compensation of interaction # 50, immediately downstream of D0 in the anti-proton direction. The beams are highly elliptical at this location and the separations are close to  $6\sigma$ . From the above discussion it is clear that the field due to the proton beam cannot be compensated by a round wire.

We therefore need to examine alternative compensation strategies. Instead of directly compensating the field, we can try to compensate some of the effects on the beam optics due to the field of the strong beam. We list here some possibilities:

1. Tune shift compensation
2. Nonlinear map minimization
3. Resonance compensation
4. Numerical optimization

The field of the strong beam also changes the closed orbit, chromaticities, and coupling but we think it unlikely that compensating these effects will reduce the diffusion significantly. In the remainder of this section, we will consider the first two strategies in detail.

#### Compensation of the tune shift and its gradient

One approach is to reduce the nonlinear tune spread induced by the beam-beam interactions. Since the largest tune shift occurs at small amplitudes, we can attempt to cancel the tune shift and its gradient at the center of the anti-proton bunch. The tune shifts at zero amplitude due to a beam-beam interaction with an elliptic beam are given by (cf. Appendix A)

$$\lim_{\substack{a_x \rightarrow 0 \\ a_y \rightarrow 0}} \Delta\nu_x = \xi_x \int_0^1 \frac{e^{-\frac{d_x^2 + f d_y^2}{2} v}}{\sqrt{v(r^2 - 1) + 1}} (1 - d_x^2 v) dv, \quad (15)$$

$$\lim_{\substack{a_x \rightarrow 0 \\ a_y \rightarrow 0}} \Delta\nu_y = \xi_y \int_0^1 \frac{e^{-\frac{d_x^2 + f d_y^2}{2} v}}{\sqrt{v(r^2 - 1) + 1}} (f - f^2 d_y^2 v) dv, \quad (16)$$

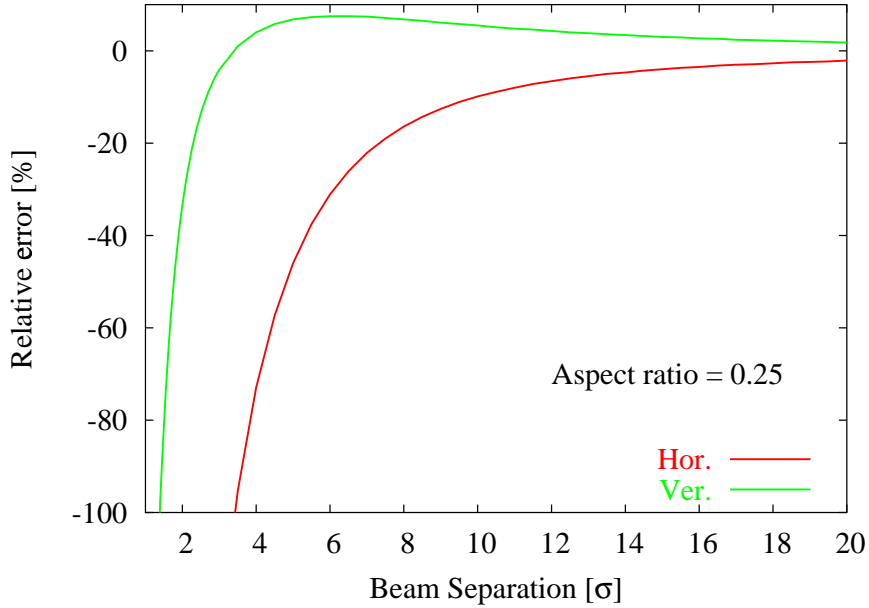


Figure 10: The relative error between the kicks of an elliptical beam with aspect ratio 0.25 and the kicks due to a wire as a function of the separation.

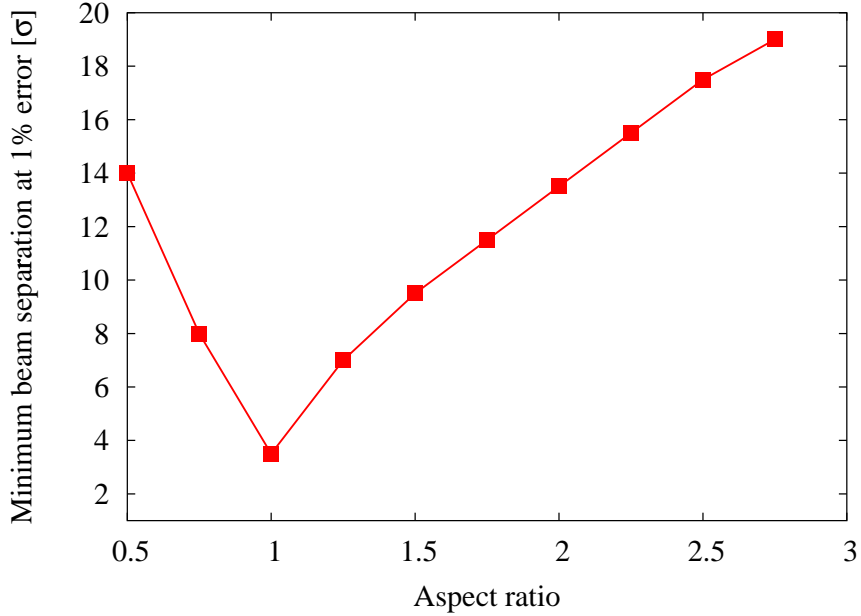


Figure 11: Minimum beam separation required to match a  $1/r$  field shown as a function of the aspect ratio of an elliptical beam. At separations above the minimum separation, the  $1/r$  field of a wire and that of the elliptical beam differ by less than 1%. If the beam sizes in the two planes differ more than a factor of 2, then the minimum beam separation exceeds  $14\sigma$ .

where

$$\xi_{x,y} = \frac{N_b r_p}{4\pi\gamma_p\varepsilon_{x,y}} > 0 \quad (17)$$

is the beam-beam parameter. The tune shifts due to a wire are given by (cf Appendix B)

$$\Delta\nu_x(W) = -\frac{\mu_0}{8\pi^2(B\rho)}\beta_x \left[ \frac{I_W L \cos 2\theta_W}{r_W^2} \right], \quad \Delta\nu_y(W) = +\frac{\mu_0}{8\pi^2(B\rho)}\beta_y \left[ \frac{I_W L \cos 2\theta_W}{r_W^2} \right] \quad (18)$$

where  $\theta_W$  is the angle of the plane of the wire,  $r_W$  is the distance of the wire from the anti-proton beam after including the closed orbit distortion caused by the wire. The tune shifts have the opposite sign and their magnitudes are given by the ratio of the beta functions at the wire. If we choose the plane of the wire to be the same as the plane of the helix, then the cancellation of one tune shift, say  $\Delta\nu_x$ , determines the radial position  $r_W$ . If instead we place the wire in the horizontal plane, the wire will be at the furthest distance while still cancelling the tune shift. The tune shifts scale as  $I_W/r_W^2$ , so doubling the separation will quadruple the current required to maintain the tune shift compensation.

We also want to compensate the gradient of the tune shift at small betatron amplitudes. From the expressions for the tune shifts due to beam-beam interactions (shown in Appendix A), it follows that all gradients of the tune shift due to beam-beam interactions vanish at zero amplitude, i.e.

$$0 = \lim_{a_x, a_y \rightarrow 0} \frac{\partial}{\partial a_x} \Delta\nu_x = \lim_{a_x, a_y \rightarrow 0} \frac{\partial}{\partial a_y} \Delta\nu_x = \lim_{a_x, a_y \rightarrow 0} \frac{\partial}{\partial a_y} \Delta\nu_y \quad (19)$$

This is also true for the gradient of the tune shifts at zero amplitudes induced by a wire. Thus the wire cannot change the gradients at the origin and the gradients vanish at zero amplitudes with and without the wire.

We chose to compensate the tune shift due to the parasitic downstream of D0. The horizontal tune-shift is one of the largest amongst the parasitics, the tune-shifts are (0.003,-0.0004) at nominal beam parameters. With the wire placed in the plane of the helix, the wire needs to be positioned at (0.315, 0.625) mm or at a separation of  $1.3\sigma$ . This separation is unrealistically small but was used in the simulation to test the principle. The beam intensity was also increased 10-fold in order to see an effect on the diffusion. Figure 12 shows the diffusion coefficients with this setting of the wire. The diffusion has increased by several orders in magnitude, especially at small amplitudes. Figure 13 shows the tune footprints with and without compensation. While the wire does compress the bulk of the tune footprint, there are several particles whose horizontal tune has moved close to 0.5. These and other particles with large tune changes contribute to the large increase in diffusion and emittance growth. Placing the wire on the x-axis to cancel the tune shift also lead to similar increases in diffusion. Thus a naive tune shift compensation does not work.

If the field profiles do not match, then we cannot compress the tune footprint due to an elliptical beam by a single round beam. Instead several round wires may be required or alternatively a wire with a different cross-section whose field matches that of the beam. We discuss these alternatives in later sections.

### Nonlinear map minimization

The principle behind this correction strategy is simple: minimize the maximum phase space distortions by finding the appropriate corrector strengths. Consider 2D phase space and a map which transports particles

$$\vec{z}_f \equiv \begin{pmatrix} x_f \\ px_f \end{pmatrix} = \mathcal{M}\vec{z}_0 = \begin{pmatrix} \sum A_{ij}x_0^i p x_0^j \\ \sum B_{ij}x_0^i p x_0^j \end{pmatrix} \quad (20)$$

$A_{ij}, B_{ij}$  are functions of the magnet and corrector strengths. The map is area-preserving which constrains the values of  $A, B$ . Minimizing the  $L_1$  vector norm of the map minimizes

$$|x_f| + |px_f| = \sum [|A_{ij}|x_0^i p x_0^j + |B_{ij}|x_0^i p x_0^j] \quad (21)$$

We can also minimize the  $L_\infty$  function norm of the phase space variables defined as

$$(\|x_f\|, \|px_f\|)_{L_\infty} = \max_{\vec{z} \in \mathcal{D}} (x_f(NL), px_f(NL)) \quad (22)$$

where e.g.  $x_f(NL)$  is the nonlinear part of  $x_f$ .

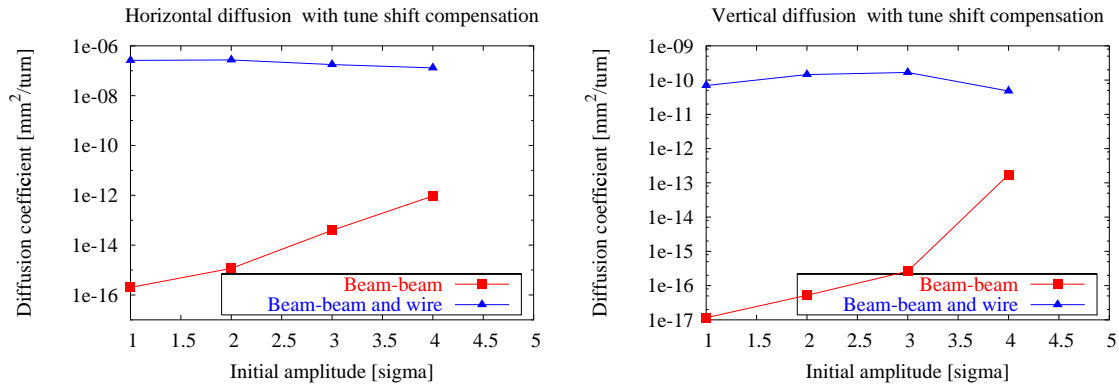


Figure 12: Horizontal and vertical diffusion coefficients for the local correction of the nearest parasitic downstream of D0 by a round wire placed to cancel the zero amplitude tune shifts.

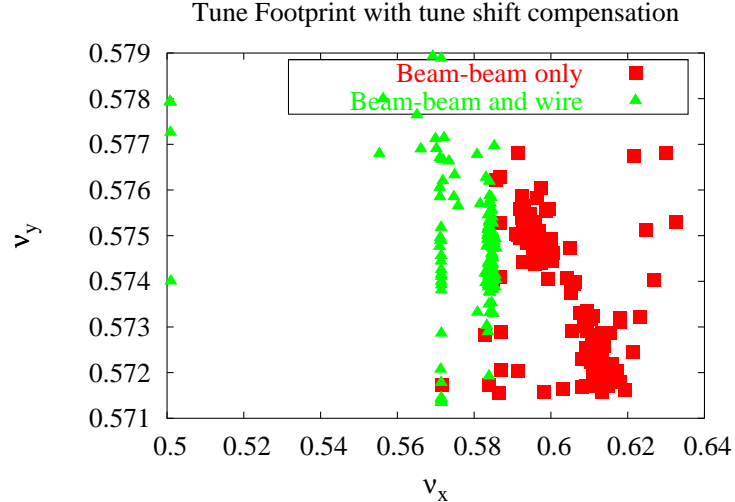


Figure 13: Tune footprints with only the beam-beam interaction downstream of D0, and the beam-beam interaction with a wire to cancel the zero amplitude tune shifts.

	Largest	Resonances $(p, q)$ at $2\sigma$
		Others
Lattice driven	$(2, -1)$	$(0, 3), (2, 1), (1, -3), (1, -2), (1, 2)$
Lattice and beam-beam driven	$(3, 4)$	$(3, 2), (1, 4), (2, 3), (5, 2), (2, 3)$

Table 1: Comparison of lattice driven and beam-beam driven resonances at 980 GeV. The beam-beam interactions drive the 7th order and the 5th order resonances strongly.

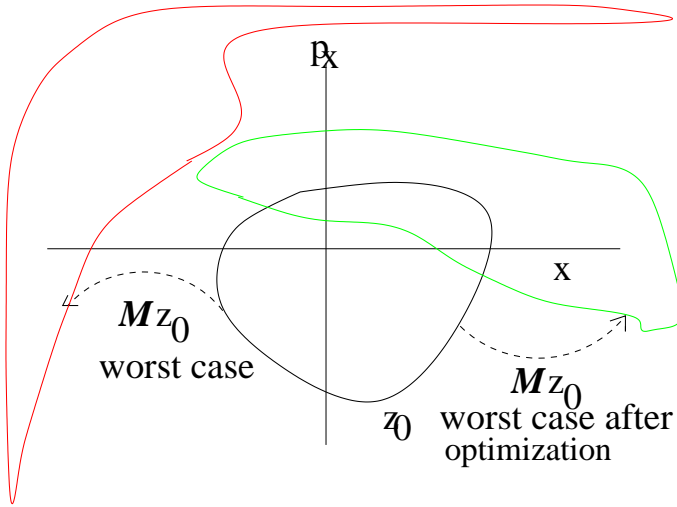


Figure 14: Cartoon of a phase space distortion minimized by appropriate choice of correctors.

the discussion of this analytical calculation in the following Section 2.4.1. There is a somewhat larger discrepancy in the currents, which probably can be attributed to the approximations made in the analytical calculation and the fact that the map was evaluated at  $1\sigma$  and not on the centroid as in the analytical case. We also checked whether the current increases linearly with increasing proton beam intensity, and indeed found to be true. Therefore, from the results obtained by two different methods, we can conclude that the best one can do with the local correction of elliptic beam-beam kicks with round wires is placing the wire to ensure that the kicks have the right orientation, and adjusting the current to match their magnitudes.

We used BBSIM to check whether this is good enough to reduce the diffusion coefficients. Unfortunately, studying the nearest parasitic downstream D0 (which showed the largest single diffusion coefficient among all parasitics) the results seem to show that the diffusion is enhanced by several orders in magnitude, hence this solution that is equivalent to matching the fields at a single amplitude is not good enough.

### Resonance compensation

A possible method to reduce the nonlinearities is to compensate selected resonances. The beam-beam interactions drive several resonances strongly. Figure 15 shows the main resonances driven by the beam-beam interactions and lattice nonlinearities at 980 GeV. Seventh and fifth order resonances driven by the long-range interactions are the strongest. Table 1 shows the dominant resonances driven by the lattice nonlinearities alone and the dominant resonances when beam-beam interactions are included.

In order to understand the resonances driven by the field of a wire, it is first useful to decompose the

Pictorially this can be represented as shown in a cartoon representation in Figure 14. Without correction, nonlinearities could in the worst case transport the original domain in phase space (black curve) to the red curve. With optimum correction by the wire, the largest excursions are limited to the green curve. Of course in practice we used 4D phase space variables.

A polynomial map to seventh order in phase space variables was computed by COSY Infinity [8]. The transverse position and current of the wire were fitted to minimize the  $L^\infty$  norm of the map with a weight of  $1\sigma$ . We obtained the following results:  $(x_{WA}, y_{WA}) = (0.539, 1.871) \text{ mm}$  and  $I = 21.758 \text{ A}$ . The positions are very close to the positions found by requiring that the field lines of the wire at the centroid of the anti-proton beam are tangential to the field lines from the elliptical proton beam - see

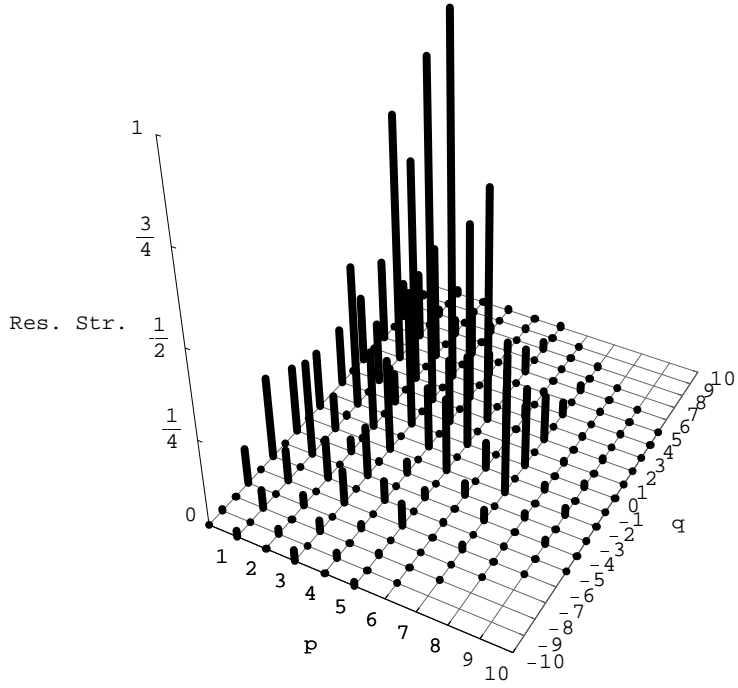


Figure 15: Resonances driven by the beam-beam interactions and the lattice nonlinearities at 980 GeV. The beam-beam interactions dominate the contributions to the resonance driving terms.

field into multipole components. From the magnetic field of a long wire,

$$B_y + iB_x = -\frac{\mu_0 I}{2\pi} \frac{1}{r_W e^{i\phi_W} - (x + iy)} \quad (23)$$

it follows that the multipole expansion of a wire is

$$B_y + iB_x = B_{0,W} \sum_{n=0}^{\infty} [b_n + ia_n] \left( \frac{x + iy}{r_W} \right)^n \quad (24)$$

where

$$B_{0,W} = \frac{\mu_0 I}{2\pi r_W}, \quad b_{n,W} = -\cos(n+1)\phi_W, \quad a_{n,W} = \sin(n+1)\phi_W \quad (25)$$

A wire has multipoles of all orders, both normal and skew. The angular position  $\phi_W$  of the wire determines the multipole coefficients to all orders. Furthermore, the skew coefficients are completely determined by the normal coefficients and vice-versa. The resonance driving terms can be determined from these multipole coefficients, see Appendix B.

It therefore follows that we can only compensate a single resonance (either normal or skew) with a single wire. Compensation of even the most dominant resonance will however change all other resonances in a determined but uncontrolled fashion. This does not seem to be a promising approach and we have not pursued it further.

### Numerical optimization

In our studies at injection energy we used a rastering technique based on short term tracking, see Section 4 for the details. This numerical method identified parameters which improved the dynamic aperture. It is possible that a similar technique would be useful at collision energy but we have not pursued it.

## 2.4 Elliptic cylindrical wires

Assume that an infinitely long wire with elliptical cross-section is given, and want to calculate the magnetic field at an arbitrary point outside the wire. Further assume that the ellipse semi-major axis is  $a$  and the semi-minor axis is  $b$  ( $a > b$ ), and the ellipse is upright, i.e. the coordinate system is chosen with the  $z$  axis parallel to the wire, and  $(x, y)$  is centered and parallel with the ellipse's principal axes. The ellipse than can be described by

$$x = a \cos t, \quad y = b \sin t, \quad (26)$$

$t \in [0, 2\pi]$  in parametric form, or as

$$\frac{x^2}{a^2} + \frac{y^2}{b^2} = 1. \quad (27)$$

We would like to produce a magnetic field with elliptic symmetry. If we employ Maxwell's equations in their boundary form,

$$B_{n_1} - B_{n_2} = 0, \quad B_{t_1} - B_{t_2} = \mu_0 J_s, \quad (28)$$

where  $J_s$  is the surface current density, the solution presents itself. Since the normal component of the field must be continuous, one way to make sure that the normal component of the field is zero outside the ellipse is to have a hollow ellipse, and than it follows from Ampère's law that the field inside the ellipse is zero, giving only a tangential component on the boundary and hence outside the ellipse, and this is what we would like to have. Therefore, we want to compute the orientation and magnitude of the field outside.

We use elliptical cylindrical coordinates  $(u, v, z)$  to take advantage of the elliptic symmetry of the problem. The relationship between Cartesian and elliptical coordinates is given by

$$x = c \cosh u \cos v, \quad y = c \sinh u \sin v, \quad z = z, \quad (29)$$

where  $u \in [0, \infty]$ ,  $v \in [0, 2\pi]$ , and  $c = \sqrt{a^2 - b^2}$ . Contours with  $u = \text{const.}$  are ellipses, and an ellipse is determined by  $\cosh u_0 = a/c$ . Therefore, in these coordinates, outside the ellipse the magnetic field is of the form

$$\vec{B} = (B_u, B_v, B_z) = (0, B_v, 0). \quad (30)$$

The length element can be shown to be

$$d\vec{l} = dx\hat{i} + dy\hat{j} + dz\hat{k} = h_u du\hat{u} + h_v dv\hat{v} + dz\hat{k}, \quad (31)$$

where

$$h_u(u, v) = h_v(u, v) = c\sqrt{\cosh^2 u - \cos^2 v}. \quad (32)$$

To compute the magnitude of the field we employ Ampère's law,

$$\oint \vec{B} \cdot d\vec{l} = \mu_0 I, \quad (33)$$

where  $I$  is the total current, obtained by integrating the surface current density. In view of the symmetry of the field, the integral becomes

$$\int_0^{2\pi} B_v h_v dv = \mu_0 I. \quad (34)$$

Recalling that the solution of Maxwell's equation is unique, finding one solution means finding the solution. A solution can be read from the equation immediately, namely

$$B_v(u, v) = \frac{\mu_0 I}{2\pi h_v(u, v)}, \quad (35)$$

which is subject to the boundary condition

$$B_v(u_0, v) = \frac{\mu_0 I}{2\pi h_v(u_0, v)}. \quad (36)$$

Therefore, the solution found is the unique solution of Maxwell's equations and satisfies the boundary condition. Utilizing the definition of the elliptical coordinates, this can be expressed as a function of  $(x, y)$ ,

$$B_v(x, y) = \frac{\mu_0 I}{2\pi \left[ c^4 - 2c^2(x^2 - y^2) + (x^2 + y^2)^2 \right]^{1/4}}. \quad (37)$$

The special case of the round wire can be obtained by setting  $c = 0$ . Also, note that at large distances the actual value of  $c$  does not really matter, and the field lines, which follow the wire contour close to the ellipse become more and more circular, resembling the field of the round wire, and the same similarity is obtained in the case of the elliptic beam-beam field lines.

However, we want the horizontal and vertical kicks, so we need the tangent vectors to the ellipse describing the field lines at an arbitrary point. This can be done by noticing that

$$\vec{B} = B_v \hat{v} = B_x \hat{i} + B_y \hat{j}, \quad (38)$$

and from the definition of the elliptical coordinates it follows that

$$\hat{v} = \frac{-\hat{i} \cosh u \sin v + \hat{j} \sinh u \cos v}{\sqrt{\cosh^2 u - \cos^2 v}}. \quad (39)$$

Therefore

$$B_x = -\frac{\mu_0 I}{2\pi} \frac{c \cosh u \sin v}{h_v^2}, \quad B_y = \frac{\mu_0 I}{2\pi} \frac{c \sinh u \cos v}{h_v^2}. \quad (40)$$

Again, it can be expressed in terms of  $(x, y)$ , and assuming  $x, y > 0$  we obtain for the kicks

$$\Delta x' = -\frac{\mu_0 I l}{2\pi (B\rho)} \frac{\sqrt{r^4 - (c^2 - h_v^2)^2}}{2ch_v^2}, \quad \Delta y' = -\frac{\mu_0 I l}{2\pi (B\rho)} \frac{(c^2 + r^2 + h_v^2) \sqrt{c^4 - (r^2 - h_v^2)^2}}{4c^2 h_v^2 x}, \quad (41)$$

where

$$r^2 = x^2 + y^2, \quad h_v^2 = \sqrt{c^4 - 2c^2(x^2 - y^2) + (x^2 + y^2)^2}. \quad (42)$$

If  $a < b$ , the results can be obtained by interchanging the two planes. For other signs of  $(x, y)$  the kicks are obtained from

$$\Delta x'(x, y) = \text{sgn}(x) \Delta x'(|x|, |y|), \quad \Delta y'(x, y) = \text{sgn}(y) \Delta y'(|x|, |y|). \quad (43)$$

The question that we have to answer now is to what degree the kick of the elliptical wire approximates the kick of an elliptical beam, since at least from the form of the kicks there is no obvious correspondence between the two. Since the compensation should work in the particular case of round beams and wires, the current and transverse position of the elliptic wire is fixed to be the same as in the case of round beam compensation. This leaves as free parameter the size of the wire ellipse. Since we want to preserve the symmetry imposed by the elliptic beam, we want to calculate a parameter  $\lambda$  such that  $(a, b) = \lambda(\sigma_x, \sigma_y)$ . By plotting the relative error in the magnitude of the kicks at a certain amplitude as a function of strong beam aspect ratio and  $\lambda$ , the minimum should correspond to the best value of  $\lambda$ . Then, we can check whether for this value of  $\lambda$  the error stays small for other amplitudes and aspect ratios. In Fig. 16 the error is evaluated at amplitudes of  $(a_x, a_y) = (3, 3)$  for aspect ratios in the range  $[0.25, 4]$ , which are the relevant aspect ratios for the Tevatron. It follows that the optimum value is  $\lambda = \sqrt{2}$ .

Now we can look at the dependence of the error on the aspect ratio. If we plot the error as a function of aspect ratio and radial amplitude  $d = \sqrt{a_x^2 + a_y^2}$  we obtain Fig. 17. As seen in Fig. 17, the error is small overall, but larger for extreme values of the aspect ratios, hence we look next for the extreme aspect ratios 0.25 and 4 at the error as a function of horizontal and vertical amplitudes in two steps: inside the beam's core and outside. The results are presented in Figs. 18 and 19.

The overall conclusion is that elliptic cylindrical wires are a very good approximation of the elliptic Gaussian beam-beam kicks outside the core of the beam. The elliptic wire behaves similarly for the elliptic beams as the round wires for the round beams. The relative error at distances larger than  $3\sigma$

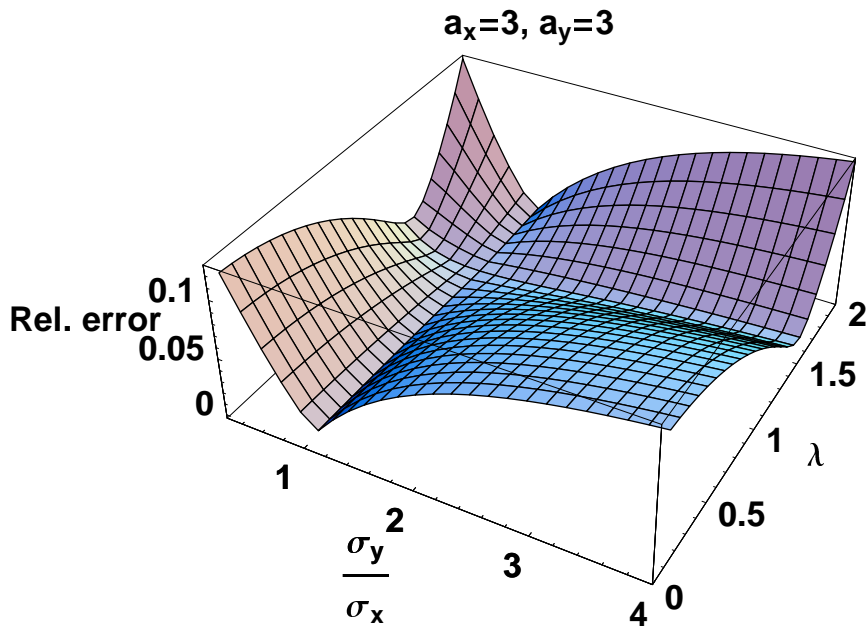


Figure 16: Relative error between the kicks at amplitude ( $a_x = 3, a_y = 3$ ) due to an elliptical wire and an elliptical beam as a function of  $\sigma_y/\sigma_x$  and a free parameter  $\lambda$ . The minimum occurs at  $\lambda = \sqrt{2}$  implying that the best values for the wire cross-section are  $(a, b) = (\sqrt{2}\sigma_x, \sqrt{2}\sigma_y)$  where  $(a, b)$  are the semi-major and semi-minor axes of the ellipse.

### Elliptical cylindric wire vs. elliptical Gaussian beams

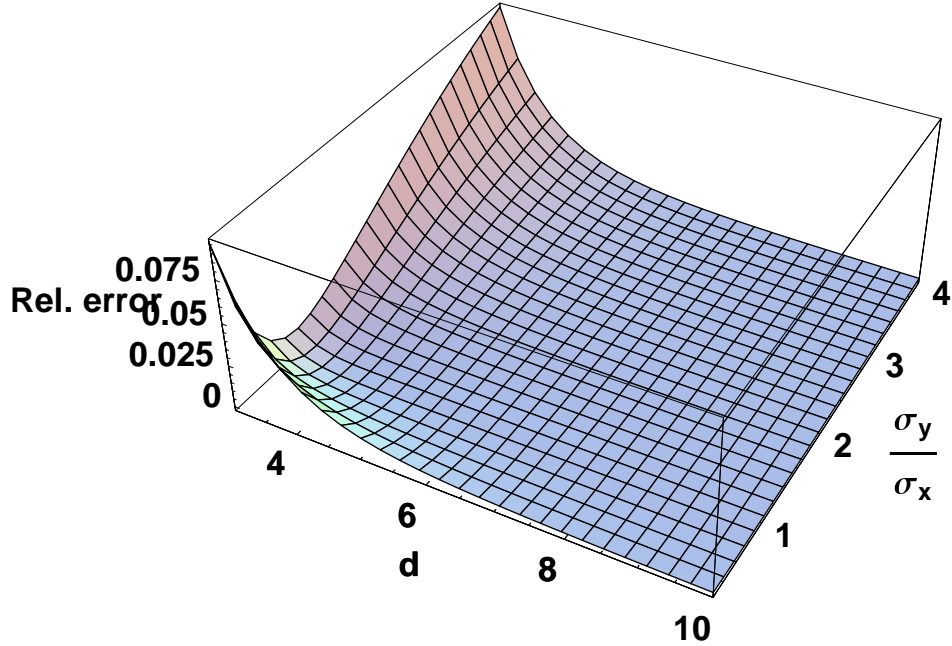


Figure 17: The relative error between an elliptical wire and elliptic beam-beam kicks as a function of aspect ratio and radial amplitude.

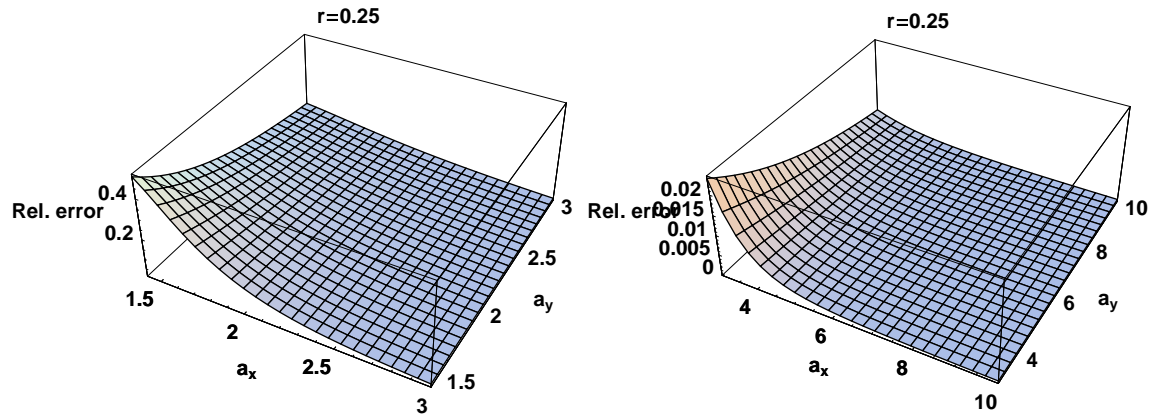


Figure 18: The relative error between an elliptical wire and elliptic beam-beam kicks as a function of amplitude  $a$ ) inside the core and b) outside the core for small aspect ratio.

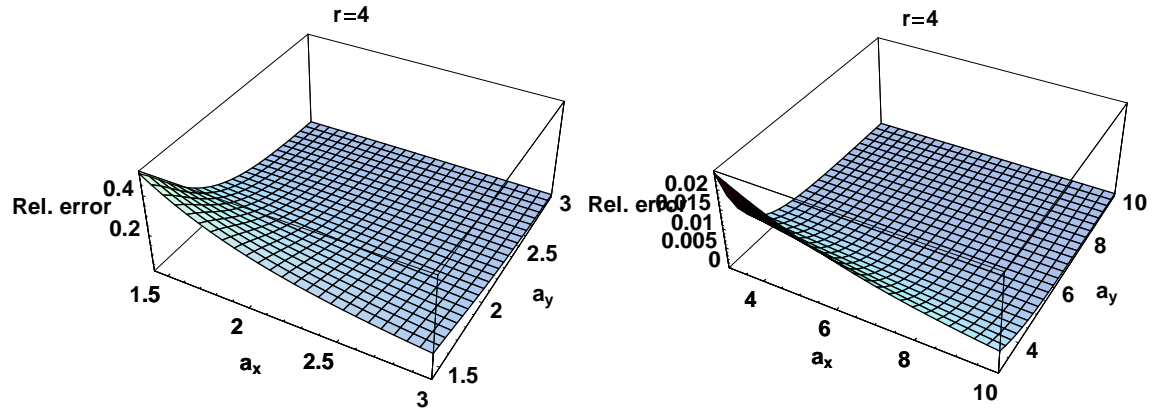


Figure 19: The relative error between an elliptical wire and elliptic beam-beam kicks as a function of amplitude  $a$ ) inside the core and b) outside the core for large aspect ratio.

from the strong beam centroid are smaller than 2% and decreasing monotonically at even larger distances. The transverse position and current of the elliptical wire are the same as in the round beam case, and the extent of the wire is related to the rms Gaussian beam sizes by  $(a, b) = (\sqrt{2}\sigma_x, \sqrt{2}\sigma_y)$ .

The elliptic cylindrical wire has only recently been implemented in the code BSSIM, so we were not able to test the efficacy of the elliptical wire in simulations.

#### 2.4.1 Approximation of the elliptical wire kicks by round wire kicks

Here we compute the best approximation of the kicks due to an elliptical wire by a round wire. We know from the previous section, that at distances larger than  $3\sigma$  the field lines of an elliptic Gaussian beam are very well approximated by elliptic wires. This is the case for all parasitics in the Tevatron. Moreover, these field lines are elliptic, and the parameters of the ellipse that passes through the centroid of the weak beam can be computed. We also know that the field lines of a round wire are circles at any distance from the wire. Therefore, the best approximation by a round wire will be such that the circular field lines of the round wire are tangent to the elliptical field lines of the beam at the location of the weak beam's centroid.

Mathematically speaking, what we need is to find the parameters of the osculating circle of an ellipse at a point, where the ellipse is the ellipse of the field lines passing through the weak beam's centroid and the point is the centroid itself. See Fig. 20. The osculating circle is the circle that is tangent to a curve at a specified point. If a planar curve is given in parametric form  $(f(t), g(t))$  and parameterized by  $t$ , then the center and radius of the osculating circle are given by

$$x = f - \frac{g'(f'^2 + g'^2)}{f'g'' - f''g'}, \quad y = g + \frac{f'(f'^2 + g'^2)}{f'g'' - f''g'}, \quad R = \frac{(f'^2 + g'^2)^{3/2}}{f'g'' - f''g'}. \quad (44)$$

The prime represents derivative with respect to  $t$ .

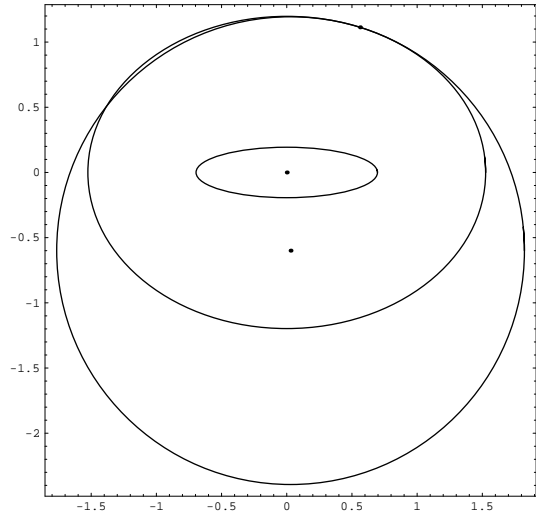


Figure 20: Osculating circle to an ellipse. The figure depicts the actual situation of the nearest parasitic beam-beam interaction downstream D0.

Fig. 20 represent the actual situation of the nearest parasitic beam-beam interaction downstream D0. The inner ellipse represents the  $1\sigma$  ( $\sigma_x = 0.696\text{mm}$ ,  $\sigma_y = 0.193\text{mm}$ ) extent of the proton beam, its centroid coincides with the dot in the ellipse's center, and it is taken as the origin. The upper dot is the anti-proton beam's centroid, the separation being  $(x_{sep}, y_{sep}) = (0.562, 1.113)\text{mm}$ . The large ellipse is the field line generated by the proton beam and passes through the anti-proton beam's centroid. The anti-proton beam centroid corresponds to  $(u, v) = (1.05804, 1.19376)$ , and the ellipse is given in parametric form by

$$x = 1.52539 \cos t, \quad y = 1.1973 \sin t. \quad (45)$$

This gives  $(x, y, R) = (0.029, -0.600, 1.794)$ . Therefore, the anti-proton-round wire distance is  $(x_{WA}, y_{WA}) = (0.532, 1.713)\text{mm}$ . This transverse placement of the wire will assure that at the location of the anti-proton beam centroid the kick will be parallel. Their magnitude can be adjusted by adjusting the current. From (4) and (37) it follows that

$$I_r = I_e \frac{\sqrt{x_{WA}^2 + y_{WA}^2}}{h_v (1.05804, 1.19376)}. \quad (46)$$

For design intensity  $N_b = 2.7 \cdot 10^{11}$ , and 1m length wires  $I_e = ecN_b = 12.968A$ , which gives  $I_r = 15.662A$ . This analytical result was compared earlier with the result obtained by map minimization in Section 2.3.1.

### 3 Non-local compensation

Up to now, the discussion centered on local correction of one parasitic beam-beam interaction by one wire. The next questions that need to be addressed are the non-local correction of a beam-beam kick by a wire, and correction of several beam-beam kicks by a or several wires. For the latter case, the concept of average kick correction will be presented.

#### 3.1 Analytical Results

If the wire is not at the same location as the beam-beam interaction, then simply cancelling the kick at a distant location is the wrong strategy. This can easily increase the phase space distortion depending on the phase advance between the beam-beam interaction and the wire. Instead we could use the wire to restore the phase space trajectories back to their original paths in the absence of the beam-beam interaction. The original trajectories, in the absence of other nonlinearities, are circles in Floquet space. We therefore transform to Floquet coordinates.

$$X = \frac{x}{\sqrt{\beta_x}}, \quad P_X = \frac{\beta_x x' + \alpha_x x}{\sqrt{\beta_x}}, \quad Y = \frac{y}{\sqrt{\beta_y}}, \quad P_Y = \frac{\beta_y y' + \alpha_y y}{\sqrt{\beta_y}} \quad (47)$$

If the motion between points 1 and 2 is purely linear, then the transformation between the Floquet coordinates between these two points is

$$\begin{pmatrix} X \\ P_X \\ Y \\ P_Y \end{pmatrix}_2 = \begin{bmatrix} R(\psi_x) & 0 \\ 0 & R(\psi_y) \end{bmatrix} \begin{pmatrix} X \\ P_X \\ Y \\ P_Y \end{pmatrix}_1 \quad (48)$$

where  $R(\psi)$  is the  $2 \times 2$  rotation matrix.

The impulsive kicks in Floquet coordinates are given by

$$\Delta P_X = \sqrt{\beta_x} \Delta x', \quad \Delta P_Y = \sqrt{\beta_y} \Delta y'$$

The beta functions that will be used are those on the *anti-proton* helix, even when scaling the coordinates of the *proton bunch*. Thus

$$X_{P0} = \frac{x_{P0}}{\sqrt{\beta_x(\bar{p})}}, \quad X_A = \frac{x_A}{\sqrt{\beta_x(\bar{p})}}, \quad Y_{P0} = \frac{y_{P0}}{\sqrt{\beta_y(\bar{p})}}, \quad Y_A = \frac{y_A}{\sqrt{\beta_y(\bar{p})}} \quad (49)$$

Defining the constants

$$C_b = \frac{2N_p r_p}{\gamma_p}, \quad C_W = \frac{\mu_0 I_W L}{2\pi (B\rho)} \quad (50)$$

the kicks due to the round beam-beam interaction and the wire can be written as

$$\begin{aligned} \Delta P_{X,b} &\simeq -C_b \frac{\beta_{x,b}(X_{P0,b} - X_{A,b})}{[\beta_{x,b}(X_{P0,b} - X_{A,b})^2 + \beta_{y,b}(Y_{P0,b} - Y_{A,b})^2]} \\ \Delta P_{Y,b} &\simeq -C_b \frac{\beta_{y,b}(Y_{P0,b} - Y_{A,b})}{[\beta_{x,b}(X_{P0,b} - X_{A,b})^2 + \beta_{y,b}(Y_{P0,b} - Y_{A,b})^2]} \end{aligned} \quad (51)$$

$$\begin{aligned} \Delta P_{X,W} &= C_W \frac{\beta_{x,W}(X_W - X_{A,W})}{[\beta_{x,W}(X_W - X_{A,W})^2 + \beta_{y,W}(Y_W - Y_{A,W})^2]} \\ \Delta P_{Y,W} &= C_W \frac{\beta_{y,W}(Y_W - Y_{A,W})}{[\beta_{x,W}(X_W - X_{A,W})^2 + \beta_{y,W}(Y_W - Y_{A,W})^2]} \end{aligned} \quad (52)$$

where  $(\beta_{x,b}, \beta_{y,b})$ ,  $(X_{P0,b}, Y_{P0,b}, X_{A,b}, Y_{A,b})$  are the beta functions and coordinates on the anti-proton helix at the beam-beam interaction while  $(\beta_{x,W}, \beta_{y,W})$ , are the beta functions,  $(X_W, Y_W)$  the wire coordinates and  $(X_{A,W}, Y_{A,W})$  the test anti-proton coordinates, all on the anti-proton helix at the wire location.

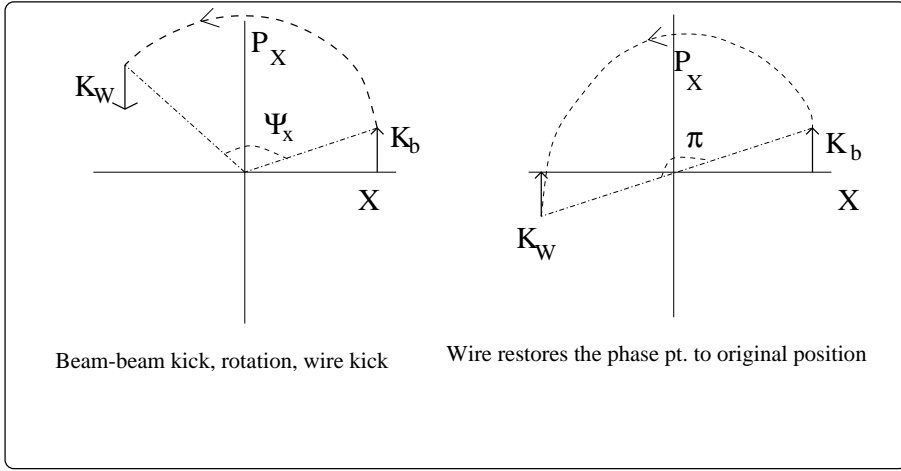


Figure 21: Phase space point following a beam-beam kick, phase rotation and followed by a wire.

### 3.1.1 One beam-beam kick

Let  $\vec{Z} = [X, P_X, Y, P_Y]^T$  denote the phase space vector in Floquet space. In this model where there is only linear motion between the beam-beam kick and the wire, the phase space vector is

$$\vec{Z}_f = K_W \odot R(\psi_x, \psi_y) \odot K_b \odot \vec{Z}_i \quad (53)$$

*Principle of Compensation:* The wire should restore the phase space trajectory to the point reached in the absence of the beam-beam interaction and the wire. In other words, the phase point after the wire is the same as though the motion were completely linear.

This requires

$$K_W \odot R(\psi_x, \psi_y) \odot K_b \odot \vec{Z}_i = R(\psi_x, \psi_y) \odot \vec{Z}_i \quad (54)$$

or equivalently

$$\sin \psi_x \Delta P_{X,b} = 0 \quad (55)$$

$$\cos \psi_x \Delta P_{X,b} + \Delta P_{X,W} = 0 \quad (56)$$

$$\sin \psi_y \Delta P_{Y,b} = 0 \quad (57)$$

$$\cos \psi_y \Delta P_{Y,b} + \Delta P_{Y,W} = 0 \quad (58)$$

Equations (55) and (57) determine the phase at which the wire should be placed. It is obvious that since the wire changes only the momenta but not the instantaneous positions, the phases should be chosen so that the positions have the values that they would in the absence of the kicks. Indeed we find  $\psi_x = m_x \pi$ ,  $\psi_y = m_y \pi$ . The other two equations (56) and (58) determine the wire parameters (current and positions) so that the momenta are also returned to their original values. *In general, this compensation only works for a specified test anti-proton.* Suppose we choose this compensation to be effective on the centroid of the anti-protons with coordinates  $(X_{A0}, P_{X,A0}, Y_{A0}, P_{Y,A0})$ .

Defining the constants

$$C_{X,A0} = -\cos \psi_x \frac{\Delta P_{X,b}(A0)}{C_W}, \quad C_{Y,A0} = -\cos \psi_y \frac{\Delta P_{Y,b}(A0)}{C_W} \quad (59)$$

the solutions for the wire positions  $(X_W, Y_W)$  are

$$X_W - X_{A0,W} = \frac{\beta_{y,W} C_{X,A0}}{\beta_{y,W} C_{X,A0}^2 + \beta_{x,W} C_{Y,A0}^2}, \quad Y_W - Y_{A0,W} = \frac{\beta_{x,W} C_{Y,A0}}{\beta_{y,W} C_{X,A0}^2 + \beta_{x,W} C_{Y,A0}^2} \quad (60)$$

This fixes the wire position in terms of the beam-beam kicks experienced by the bunch centroid. It places no restriction as yet on the wire current or other optics constraints at the location of the wire.

The conditions that the compensation works for any other particle with Floquet coordinates  $(X_{A,W}, Y_{A,W})$  in the anti-proton bunch are

$$X_W - X_{A,W} = \frac{\beta_{y,W} C_{X,A}}{\beta_{y,W} C_{X,A}^2 + \beta_{x,W} C_{Y,A}^2}, \quad Y_W - Y_{A,W} = \frac{\beta_{x,W} C_{Y,A}}{\beta_{y,W} C_{X,A}^2 + \beta_{x,W} C_{Y,A}^2} \quad (61)$$

where the position of the wire  $(X_W, Y_W)$  is determined by Equation (60). If  $\beta_{y,W}/\beta_{x,W} = \beta_{y,b}/\beta_{x,b}$ , then the equality to be satisfied is

$$\frac{1}{C_r \cos \psi_x} [X_{A,b} - X_{A0,b}] = X_{A,W} - X_{A0,W} = \cos(\psi_x) [X_{A,b} - X_{A0,b}] \quad (62)$$

This is true if  $C_r \equiv C_b/C_W = 1$ . The same condition is obtained by requiring that the compensation is exact in the vertical plane for all particles. Hence *the three conditions for the compensation to be exact for all particles are*

$$\psi_x = m_x \pi, \quad \psi_y = m_y \pi \quad (63)$$

$$\frac{\beta_{y,W}}{\beta_{x,W}} = \frac{\beta_{y,b}}{\beta_{x,b}} \quad (64)$$

$$\frac{2N_p r_p}{\gamma_p} = \frac{\mu_0 I_W L}{2\pi (B\rho)} \Rightarrow e c N_p = I_W L \quad (65)$$

The first condition states that the compensation can only be effective if the wire is at an integer multiple of  $\pi$  away in phase in both planes. This is a very restrictive condition. The second condition requires that the beta functions at the wire have to be in the same ratio as at the beam-beam interaction. The third condition determines the integrated wire strength in terms of the bunch current.

### 3.1.2 Two beam-beam interactions compensated by a single wire

Consider for simplicity that two beam-beam interactions will be compensated by a single wire. The phase advances between the successive beam-beam kicks are  $(\psi_{x,1}, \psi_{y,1})$  and the phase advances from the 2nd beam-beam kick to the wire are  $(\psi_{x,2}, \psi_{y,2})$ .

Applying the same principle of compensation that the wire should restore the phase space point back to the circle after the wire, the compensation condition is

$$K_W \odot R(\psi_{x,2}, \psi_{y,2}) \odot K_{b2} \odot R(\psi_{x,1}, \psi_{y,1}) \odot K_{b1} \vec{Z}_i = R(\sum \psi_x, \sum \psi_y) \odot \vec{Z}_i \quad (66)$$

or equivalently

$$\sin \sum \psi_x \Delta P_{X,b1} + \sin \psi_{x,2} \Delta P_{X,b2} = 0 \quad (67)$$

$$\cos \sum \psi_x \Delta P_{X,b1} + \cos \psi_{x,2} \Delta P_{X,b2} + \Delta P_{X,W} = 0 \quad (68)$$

$$\sin \sum \psi_y \Delta P_{Y,b1} + \sin \psi_{y,2} \Delta P_{Y,b2} = 0 \quad (69)$$

$$\cos \sum \psi_y \Delta P_{Y,b1} + \cos \psi_{y,2} \Delta P_{Y,b2} + \Delta P_{Y,W} = 0 \quad (70)$$

Solving for the phases  $(\psi_{x,2}, \psi_{y,2})$  to the wire, we find

$$\tan \psi_{x,2} = -\frac{\sin \psi_{x,1}}{[\cos \psi_{x,1} + \Delta P_{x,b2}/\Delta P_{x,b1}]}, \quad \tan \psi_{y,2} = -\frac{\sin \psi_{y,1}}{[\cos \psi_{y,1} + \Delta P_{y,b2}/\Delta P_{y,b1}]} \quad (71)$$

*It is no longer necessary that the phase advance from the first beam-beam kick to the wire be a multiple of  $\pi$ .*

If we define the difference in positions between the anti-proton and the proton centroid at each beam-beam interaction as e.g.

$$\Delta X_{A,b1} = X_{P0,b1} - X_{A,b1}, \quad \Delta Y_{A,b1} = Y_{P0,b1} - Y_{A,b1} \quad (72)$$

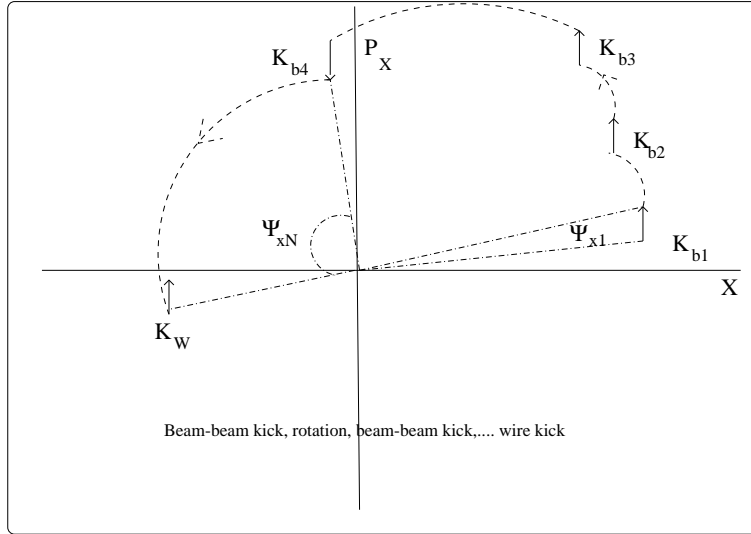


Figure 22: Phase space point following several beam-beam kicks, phase rotation between these kicks and ending up at a wire.

for the separations at the first interaction  $b1$  and similarly for the interaction  $b2$  and also define

$$C_{X,A} \equiv \frac{C_{b1}}{C_W} \frac{\cos \sum \psi_x \beta_{x,b1} \Delta X_{A,b1}}{[\beta_{x,b1} \Delta X_{A,b1}^2 + \beta_{y,b1} \Delta Y_{A,b1}^2]} + \frac{C_{b2}}{C_W} \frac{\cos \psi_{x,2} \beta_{x,b2} \Delta X_{A,b2}}{[\beta_{x,b2} \Delta X_{A,b2}^2 + \beta_{y,b2} \Delta Y_{A,b2}^2]} \quad (73)$$

$$C_{Y,A} \equiv \frac{C_{b1}}{C_W} \frac{\cos \sum \psi_y \beta_{y,b1} \Delta X_{A,b1}}{[\beta_{x,b1} \Delta X_{A,b1}^2 + \beta_{y,b1} \Delta Y_{A,b1}^2]} + \frac{C_{b2}}{C_W} \frac{\cos \psi_{y,2} \beta_{y,b2} \Delta Y_{A,b2}}{[\beta_{x,b2} \Delta X_{A,b2}^2 + \beta_{y,b2} \Delta Y_{A,b2}^2]} \quad (74)$$

then the position of the wire required to compensate the kicks on the chosen anti-proton is given by a similar expression as for a single beam-beam kick

$$X_W - X_{A,W} = \frac{\beta_{y,W} C_{X,A}}{\beta_{y,W} C_{X,A}^2 + \beta_{x,W} C_{Y,A}^2}, \quad Y_W - Y_{A,W} = \frac{\beta_{x,W} C_{Y,A}}{\beta_{y,W} C_{X,A}^2 + \beta_{x,W} C_{Y,A}^2} \quad (75)$$

This only guarantees that the beam-beam kicks will be compensated for the chosen anti-proton. The conditions for the compensation to work for all anti-protons are much more complicated than with the single beam-beam interaction. It is very likely that these conditions cannot be satisfied for all particles but we have not proven this definitively.

### 3.1.3 Several beam-beam interactions compensated by a single wire

The generalization to  $N$  kicks followed by a single wire is straightforward. Figure 22 shows the schematics. The phase advances to the wire  $(\psi_{x,N}, \psi_{y,N})$  from the  $N$ 'th beam-beam kick are given by

$$\tan \psi_{x,N} = - \frac{\sin [\sum_{i=1}^{N-1} \psi_{x,i}] \Delta P_{X,1} + \sin [\sum_{i=2}^{N-1} \psi_{x,i}] \Delta P_{X,2} + \dots + \sin [\psi_{x,N-1}] \Delta P_{X,N-1}}{\left[ \cos [\sum_{i=1}^{N-1} \psi_{x,i}] \Delta P_{X,1} + \cos [\sum_{i=2}^{N-1} \psi_{x,i}] \Delta P_{X,2} + \dots + \cos [\psi_{x,N-1}] \Delta P_{X,N-1} + \Delta P_{X,N} \right]} \quad (76)$$

$$\tan \psi_{y,N} = - \frac{\sin [\sum_{i=1}^{N-1} \psi_{y,i}] \Delta P_{Y,1} + \sin [\sum_{i=2}^{N-1} \psi_{y,i}] \Delta P_{Y,2} + \dots + \sin [\psi_{y,N-1}] \Delta P_{Y,N-1}}{\left[ \cos [\sum_{i=1}^{N-1} \psi_{y,i}] \Delta P_{Y,1} + \cos [\sum_{i=2}^{N-1} \psi_{y,i}] \Delta P_{Y,2} + \dots + \cos [\psi_{y,N-1}] \Delta P_{Y,N-1} + \Delta P_{Y,N} \right]} \quad (77)$$

Description	Longitudinal position [m]
Nearest parasitic	4248.095
$\pi$ ahead on average	4355.958
$\pi$ back on average	4020.982
$\pi$ ahead horizontal	4390.120
$\pi$ ahead vertical	4321.700
$\pi$ back horizontal	4051.845
$\pi$ back vertical	3990.118

Table 2: Conversion between phase advances and longitudinal positions for the case of the nearest parasitic downstream D0.

The coefficients  $C_{X,A}, C_{Y,A}$  are defined as

$$C_{X,A} = \frac{C_{b1}}{C_W} \frac{\cos[\sum_{i=1}^N \psi_{x,i}] \beta_{x,b1} \Delta X_{A,b1}}{[\beta_{x,b1} \Delta X_{A,b1}^2 + \beta_{y,b1} \Delta Y_{A,b1}^2]} + \frac{C_{b2}}{C_W} \frac{\cos[\sum_{i=2}^N \psi_{x,i}] \beta_{x,b2} \Delta X_{A,b2}}{[\beta_{x,b2} \Delta X_{A,b2}^2 + \beta_{y,b2} \Delta Y_{A,b2}^2]} + \dots + \frac{C_{bN}}{C_W} \frac{\cos[\psi_{x,N}] \beta_{x,bN} \Delta X_{A,bN}}{[\beta_{x,bN} \Delta X_{A,bN}^2 + \beta_{y,bN} \Delta Y_{A,bN}^2]} \quad (78)$$

$$C_{Y,A} = \frac{C_{b1}}{C_W} \frac{\cos[\sum_{i=1}^N \psi_{y,i}] \beta_{y,b1} \Delta Y_{A,b1}}{[\beta_{x,b1} \Delta X_{A,b1}^2 + \beta_{y,b1} \Delta Y_{A,b1}^2]} + \frac{C_{b2}}{C_W} \frac{\cos[\sum_{i=2}^N \psi_{y,i}] \beta_{y,b2} \Delta Y_{A,b2}}{[\beta_{x,b2} \Delta X_{A,b2}^2 + \beta_{y,b2} \Delta Y_{A,b2}^2]} + \dots + \frac{C_{bN}}{C_W} \frac{\cos[\psi_{y,N}] \beta_{y,bN} \Delta Y_{A,bN}}{[\beta_{x,bN} \Delta X_{A,bN}^2 + \beta_{y,bN} \Delta Y_{A,bN}^2]} \quad (79)$$

The solutions for the wire position are then those given in Equation (75).

It is almost certainly true that choosing the wire location by satisfying the conditions for a chosen anti-proton, e.g. at the origin, will not restore the phase space trajectories of other particles. Instead we should interpret the kicks as averaged over the anti-proton bunch distribution  $\rho_A$ , e.g.

$$\langle \Delta P_X \rangle = \int \Delta P_X \rho_A dX dY dP_x dP_y \quad (80)$$

These averaged kicks are evaluated in Appendix C.

Analogous to typical nonlinear chromaticity compensation schemes, it will be more efficient to lump several beam-beam kicks in blocks of integer multiples of  $\pi$ . Each block would be compensated by one or more wires at the appropriate location. Thus the compensation of all the beam-beam interactions will require wires at several locations.

### 3.2 Simulation Results

In this section the attempts to correct beam-beam interactions with wires placed at different longitudinal locations are summarized. According to the theory of non-local compensation of a single beam-beam kick, the longitudinal placement of the wire has well-defined values determined in terms of phase advances, namely it should be placed at  $\pi$  phase differences in both the horizontal and vertical planes with respect to the phase at which the beam-beam interaction occurs. We continued to look at the nearest parasitic downstream D0 to study this possibility. Unfortunately, the lattice of the Tevatron is such that the longitudinal locations of the  $\pi$  phase advances in each plane corresponds to different positions. We developed several Mathematica notebooks that allow us to calculate what longitudinal positions correspond to desired phases, and interpolate the optics functions corresponding to any longitudinal coordinate. Table 2 summarizes the results for the nearest parasitic downstream D0 (the longitudinal positions are with respect to B0, in the direction of the  $\bar{p}$  trajectories).

As one can see from the table, the difference between the desired positions in the horizontal and vertical planes is considerable, translating to phase errors of up to  $40^\circ$ . Under these circumstances, we placed the wire longitudinally at the location of the desired phase advance on average, and proceeded to

Description	Map norm @ 1 $\sigma$ [x10 <sup>8</sup> ]	Wire parameters		
		I [A]	x [mm]	y [mm]
Nearest parasitic (no wire)	7.56			
$\pi$ ahead on average	7.30	0.550	-0.565	-1.272
$\pi$ back on average	7.36	1.433	1.112	0.583
$\pi$ ahead horizontal	7.45	19.051	-0.928	-1.136
$\pi$ ahead vertical	7.47	8.566	-0.784	-1.093
$\pi$ back horizontal	7.43	2.221	2.004	0.265
$\pi$ back vertical	7.51	13.312	1.529	0.834

Table 3: Results of the map minimization for the case of the nearest parasitic downstream D0.

find the optimum transverse position and current by map minimization, analogously to the case of the local correction, where the map minimization produced very good results. The results are contained in Table 3. The first row is the norm of the map of the beam-beam kick only. After extensive optimization, using several algorithms (simplex, LMDIF, simulated annealing) and various initial conditions the results are not satisfactory. The map norm, even in the best of cases, decreases by not more than 4 %. This is to be compared with the case of the local correction, where the improvement in the map norm was up to two orders of magnitude, and even that improvement did not materialize in reduced diffusion coefficients. Indeed, this is what we noticed in this case too: the diffusion coefficients in some cases became several orders of magnitudes larger with wire than without wire.

In terms of diffusion coefficients, a representative case is to compare the coefficients without wire and with wire placed average  $\pi$  ahead at several amplitudes. As shown in Figure 23, the wire makes things worse. If we compare the diffusion coefficients of the case with wire placed average  $\pi$  ahead and horizontal  $\pi$  ahead, as in Figure 24, we notice that indeed in general the right phase relationship to the location of the beam-beam kick benefits the diffusion coefficients, but still not enough to actually make an improvement.

In order to keep the compensation as local as possible, we did not try locations much further away from the location of the beam-beam kick, but limited scans in longitudinal and transverse directions revealed no improvement in the results. The best solution was always found in the vicinity of the beam-beam kick, and the results start to deteriorate as the wire is moved away from the beam-beam kick, with only slight improvements in the regions of favorable phase advances.

In the next series of runs we studied whether the compensation by a single wire works better for the case when the effects of two nearest parasitics compound. These nearest parasitics do not add up coherently, since the phase advance between them is not a multiple of  $2\pi$  and the transverse locations are also different. The correction method we used is the map minimization combined with the principle of the average kick compensation, namely the wire parameters are chosen in such a way that it compensates the average kick felt by the anti-proton beam due to the two nearest parasitics. Since the phase is determined only modulo  $2\pi$ , we also tried locations at phases which are  $2\pi$  away; the longitudinal positions are in Table 4. Moreover, all four nearest parasitics were similarly studied, assuming that the correction is attempted by two wires, one close to D0 and one close to B0. The map minimization results are contained in Table 5.

The results show that even with a small current, the map norm can be reduced by up to 25-35 %. The best case is the average kick compensation, which for both IPs fall between the nearest parasitics. Despite this encouraging result, the diffusion coefficients do not improve. Some comparisons of diffusion coefficients with and without wire are shown in Figures 25-27. The intensities have been artificially increased to enhance diffusion, in order to better see the effects.

Therefore, it seems that there is no straightforward relationship between map norm and diffusion coefficients when it comes to nonlocal compensation. Since the correction, when it works, seems to be robust, these results cannot be explained in terms of small differences between the codes utilized in map minimization and tracking, respectively. The results obtained for the local compensation hint to the possibility that there is a long-term effect which contributes significantly to the outcome in terms of diffusion coefficients, but which is not captured easily in terms of maps and map norms. Despite this negative result, it is interesting to notice that while the two nearest parasitics around each IP do not

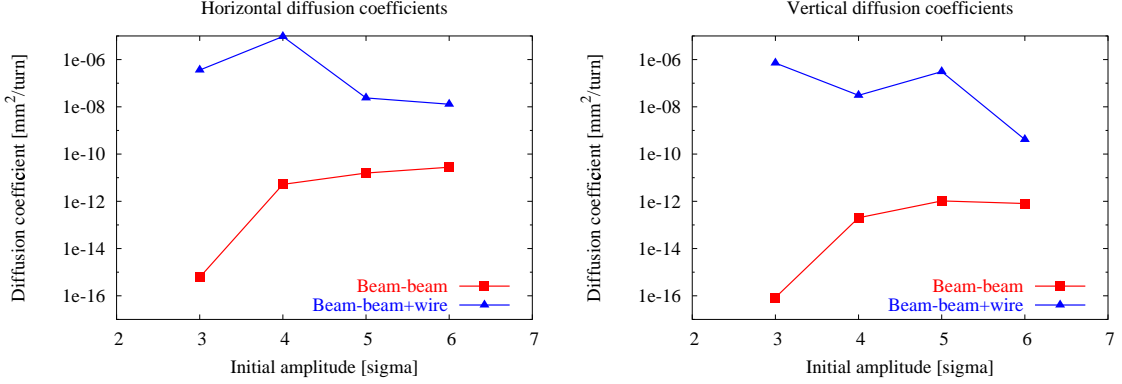


Figure 23: Horizontal and vertical diffusion coefficients of the nearest parasitic downstream D0, without wire and with wire placed average  $\pi$  ahead.

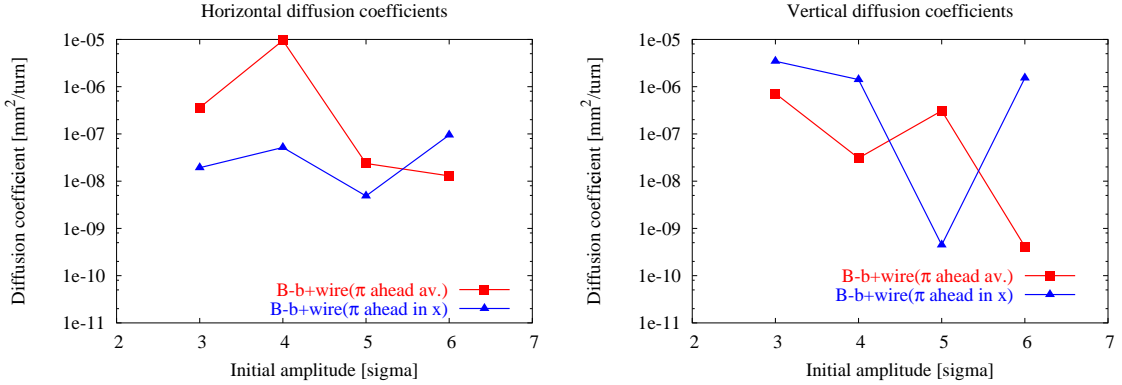


Figure 24: Horizontal and vertical diffusion coefficients of the nearest parasitic downstream D0, with wire placed average  $\pi$  ahead and horizontal  $\pi$  ahead, respectively.

Description	Longitudinal position [m]
2 NP @ D0	4129.543, 4248.095
average	4222.96
$2\pi$ ahead	4535.81
$2\pi$ back	4081.76
2 NP @ B0	6223.952, 59.275
average	6252.86
$2\pi$ ahead	50.53
$2\pi$ back	6000.32

Table 4: Longitudinal positions for the case of the nearest parasitics and the locations of the wires for average kick compensation.

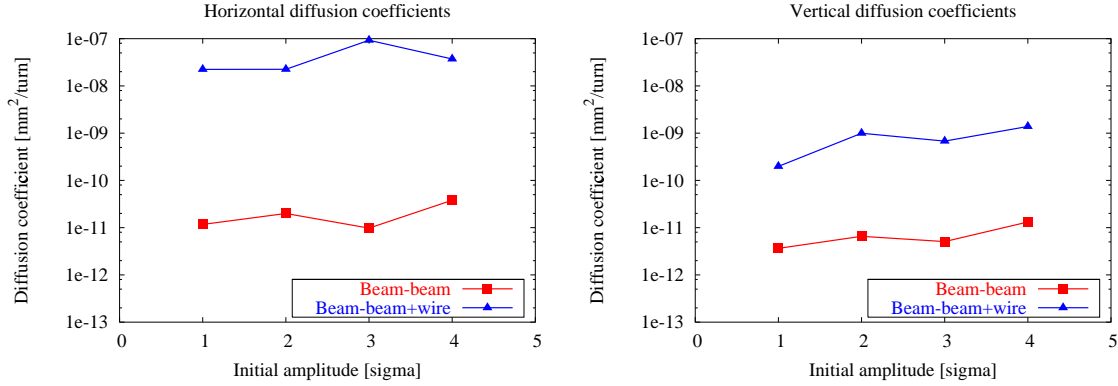


Figure 25: Horizontal and vertical diffusion coefficients of the two nearest parasitics to D0, without wire and with wire placed to cancel the average kick felt by the anti-proton beam.

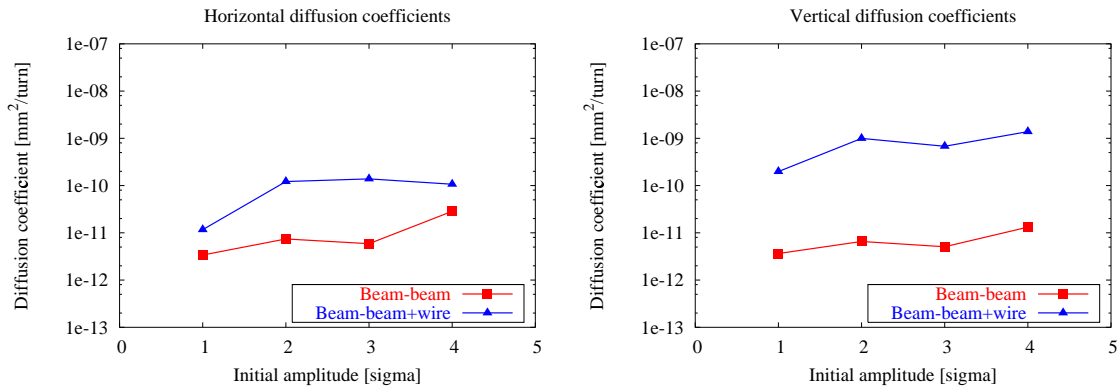


Figure 26: Horizontal and vertical diffusion coefficients of the two nearest parasitics to B0, without wire and with wire placed to cancel the average kick felt by the anti-proton beam.

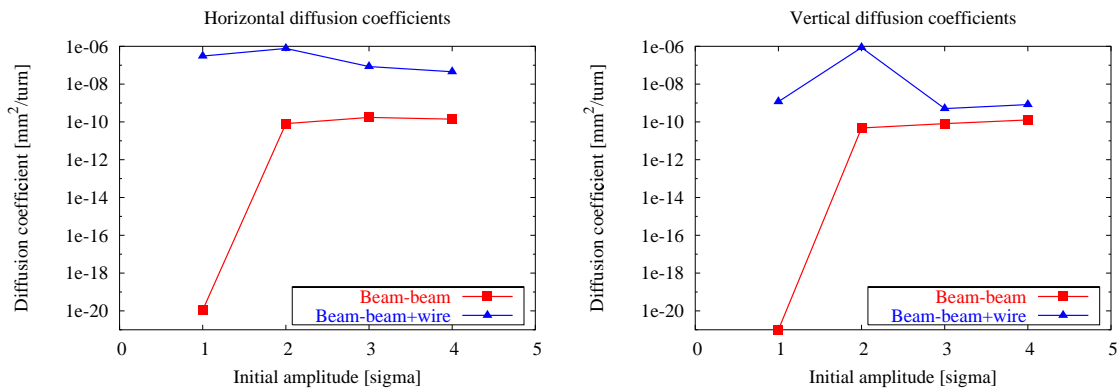


Figure 27: Horizontal and vertical diffusion coefficients of all four nearest parasitics, without wire and with two wires (one close to B0 and one close to D0) placed to cancel the average kick felt by the antiproton beam.

Description	Map norm @ 1 $\sigma$ [ $\times 10^8$ ]	Wire parameters		
		$I$ [A]	$x$ [mm]	$y$ [mm]
2 NP @ D0 (no wire)	11.40			
Average kick correction	9.13	-1.729	-1.454	1.228
2 $\pi$ ahead	11.30	17.191	2.599	0.260
2 $\pi$ back	10.70	11.521	2.184	0.072
2 NP @ B0 (no wire)	11.70			
Average kick correction	8.51	3.385	0.244	-3.344
2 $\pi$ ahead	8.77	-5.010	-1.767	0.616
2 $\pi$ back	11.50	2.627	1.974	0.116

Table 5: Results of the map minimization for the case of the nearest parasitics.

seem to compensate each other, in the case of all four nearest parasitics the small amplitude diffusion coefficient drops to practically zero.

## 4 Studies at Injection Energy

At injection energy we followed a different approach. We used the MAD model which includes all known lattice nonlinearities, and as figure of merit we used the dynamic aperture (DA). Also, a more realistic approach has been considered for the wires: we set the length of the wires to 1m, the number of wires to four, and placed them in long drifts available in the Tevatron, where the proton and anti-proton beams are well separated in order to reduce as much as possible the effect of the wires on the protons. Also, we wanted the wires to be placed at a reasonable distance from the anti-proton beam in order to allow for orbit drifts and manipulations. Therefore, we placed the wires in the sections A17, C0, E0, and F0.

First we used a rastering technique to find the optimum setting. We scanned in transverse position of the wires (radius and angle) followed by scans in the current one wire at a time in order to maximize the short term ( $10^4$  turns) DA, using the code Sixtrack [9], which is a fast symplectic tracking code. We incorporated a symplectic wire module in order to study the DA with wires and beam-beam. As a test case, we used anti-proton bunch #1.

We also used polynomial maps generated by COSY Infinity to reduce the map norm, similar to the procedure followed for collision energy. At low orders the map optimizers resulted in values for currents that worsened the DA. It follows that low orders of the map do not determine the DA and/or the wires enhance the nonlinearities. At seventh order the norm of the map stabilized, and optimization gives values close to those obtained by rastering. Tables 6 and 7 show the changes in the map norm, the

Case	Map norm (order 7) [ $\times 10^3$ ]	Max. res. str. [ $\times 10^9$ ]	Res.
No beam-beam, no wires	4.68	2.26	(1, -1)
Beam-beam on, no wires	4.85	60.2	(1, -1)
No beam-beam, best wires	4.70	4.35	(1, -1)
Beam-beam on, best wires	4.86	19.0	(1, -1)

Table 6: Norm of the map and the dominant resonance with and without wires. The linear coupling resonance was the dominant resonance.

Case	Largest 5th order	Max. amp.	Largest 7th order	Max. amp.
bb on, no wires	(1, 4) (3, 2) (4, 1)	$1.37 \times 10^{-9}$	(4, 3) (1, -6) (5, 2)	$0.376 \times 10^{-9}$
bb on, best wires	(3, 2) (1, 4) (2, 3)	$1.16 \times 10^{-9}$	(4, 3) (3, 4) (2, 5)	$0.335 \times 10^{-9}$

Table 7: Largest 5th and 7th order resonances with and without the wires.

largest resonance which turned out to be the linear coupling resonance and the largest 5th and 7th order resonances without wires and with the best wire settings found by the rastering technique. We observe that the norm of the map is less sensitive than resonance strengths to the presence of the beam-beam interactions. The largest change was in the coupling resonance strengths which increased significantly in the presence of the beam-beam interactions. The wires reduced the strength of this coupling resonance by a factor of 3. On the other hand, the wires reduced the 5th and 7th order resonances only at the level of 10-15%. Figure 28 shows the tune footprints with and without the wires at their optimum setting. The footprint is slightly larger with the wires showing that it is not necessary to compress the tune footprint to improve the DA.

When the parameters of all four wires had been optimized by the rastering described above, the long term ( $10^6$  turns) DA was estimated by Sixtrack. The results are contained in Table 8. The long-term DA increased by almost  $2\sigma$ . The wire parameters that achieved this result are presented in Table 9. Since the lattice included other nonlinearities than the beam-beam, an independent check of the solution has been performed by F. Zimmermann of CERN using another code [5], but neglecting all nonlinearities except the beam-beam. He found that the DA increased vertically by roughly  $1.5\sigma$  for these wire parameters.

Moreover, these results are not very sensitive to placement and current of the wires. For example a  $\pm 0.5\text{mm}$  offset in the wire transverse position did not alter the DA. The same is true for small static errors in the current values. Therefore, these results seem to show that in principle an improvement is feasible by current carrying wires, but a simple rule for their placement and current does not seem to be

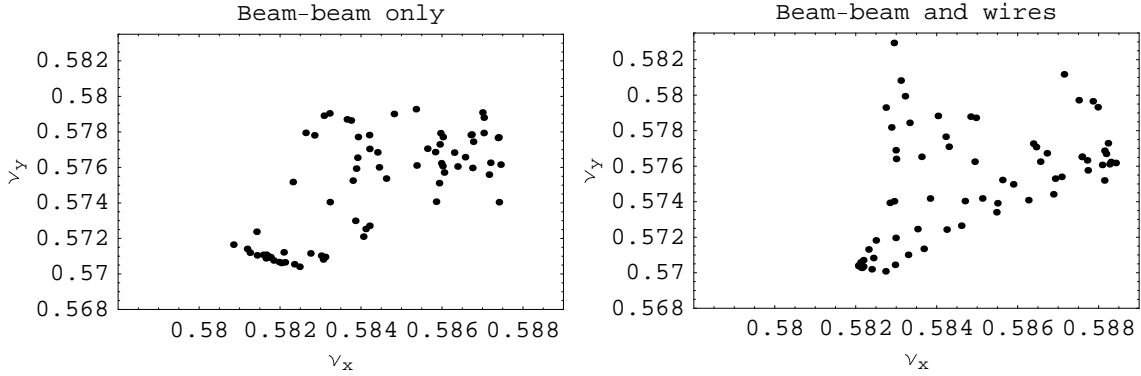


Figure 28: Tune footprints with only the beam-beam interactions (left panel) and with best setting of the wire parameters (right panel). The compensation increased the footprint slightly.

straightforward.

DA [ $\sigma$ ]	Number of turns		
	$10^4$	$10^5$	$10^6$
Beam-beam on, no wires	6.0	4.0	<b>3.7</b>
Beam-beam on, best case wires	7.0	6.5	<b>5.5</b>

Table 8: At injection energy, using 4 wires and optimizing each of them individually by rastering we obtained an improvement of the DA by almost  $2\sigma$ .

Wire	$I$ [A]	$x$ [mm]	$y$ [mm]
<b>WA17</b>	50	16.823	-1.033
<b>WC0</b>	75	12.993	-11.028
<b>WE0</b>	-25	21.232	14.282
<b>WF0</b>	232	14.004	-9.134

Table 9: The parameters of the 4 wires for which we obtained the improved DA shown in Table 8.

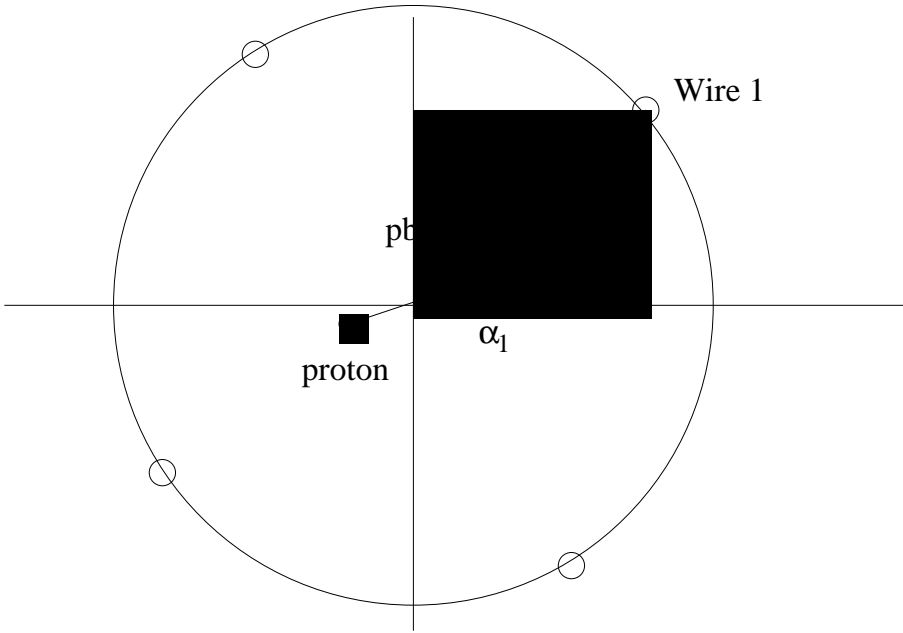


Figure 29: Geometry of several wires around the beam pipe circumference.

## 5 Multiple wires at a single location

Until this point we have considered only a single wire at each location. The possibility of installing several wires around the beam-pipe circumference increases the power of the compensation. For example, multiple wires could be used to minimize the norm of the nonlinear map at several amplitudes which could lead to reduced diffusion and emittance growth. Alternatively, they could be used to compensate several resonances simultaneously - more on this below. Multiple wires would be essential if the compensation is required both at injection and collision since the helix changes polarity during the beta squeeze. They would also adapt to future changes in the helix at any stage. This could be done for example by installing several wires around the circumference and then powering a select few optimized for the particular helix. There are also several concerns and drawbacks with multiple wires. If the compensation is required to act on the anti-protons, they may have undesired effects on the protons or vice-versa. They may also introduce aperture limitations, especially at injection when the helix is bigger. Impedances of these structures may also be an issue. These wires when powered will exert forces on each other so the wire support structures must provide adequate bracing. Finally they add to the complexity of operation and possibly the likelihood of failures. All of these concerns can be addressed with proper designs.

We now illustrate how multiple wires could be used. First we write down the field and multipole expansion with multiple wires. Figure 29 shows a sketch of wires placed around the circumference. The variables  $r_1, \phi_1$  are the radial distance and angle of wire 1 with respect to the anti-proton bunch and similarly for other wires.  $r_C$  is the radius of the cylindrical cage on which the wires are installed while  $(r_{\bar{p}}, \theta_{\bar{p}})$  are the coordinates of the anti-proton bunch relative to the center of the beam-pipe. If there are  $N_W$  wires with currents  $I_j, j = 1, \dots, N_W$ , the field of these wires can be expanded in the form (assuming each is “infinitely long”),

$$B_y + iB_x = \frac{\mu_0}{2\pi} \sum_{j=1}^{N_W} \sum_{n=0}^{\infty} I_j [-\cos(n+1)\phi_j + i \sin(n+1)\phi_j] \left[ \frac{(x+iy)^n}{r_j^{(n+1)}} \right] \quad (81)$$

where

$$\begin{aligned} r_j &= [(r_C \cos \alpha_j - r_{\bar{p}} \cos \theta_{\bar{p}})^2 + (r_C \sin \alpha_j - r_{\bar{p}} \sin \theta_{\bar{p}})^2]^{1/2} \\ \phi_j &= \arctan \left[ \frac{(r_C \sin \alpha_j - r_{\bar{p}} \sin \theta_{\bar{p}})}{(r_C \cos \alpha_j - r_{\bar{p}} \cos \theta_{\bar{p}})} \right] \end{aligned} \quad (82)$$

From the usual multipole expansion

$$B_y + iB_x = B_0 \sum_{n=0}^{\infty} (b_n + ia_n) \left[ \frac{x+iy}{R_{ref}} \right]^n \quad (83)$$

it follows that the multipole coefficients can be identified as

$$b_n = - \sum_{j=1}^{N_W} \cos(n+1)\phi_j \left[ \frac{\langle r_W \rangle}{r_j} \right]^{n+1} \frac{I_j}{\langle I_W \rangle}, \quad a_n = \sum_{j=1}^{N_W} \sin(n+1)\phi_j \left[ \frac{\langle r_W \rangle}{r_j} \right]^{n+1} \frac{I_j}{\langle I_W \rangle} \quad (84)$$

where the main field  $B_0$  and reference radius are

$$B_0 = \frac{\mu_0}{2\pi} \frac{\langle I_W \rangle}{\langle r_W \rangle}, \quad R_{ref} = \langle r_W \rangle = \frac{1}{N_W} \sum_j r_j, \quad \langle I_W \rangle = \frac{1}{N_W} \sum_j I_j \quad (85)$$

If the multiple wires are to be used for a local compensation, it could be done by choosing the wire parameters  $I_j, \phi_j$  and the number of wires to compensate the kicks  $\Delta x', \Delta y'$  over the bunch distribution from the selected beam-beam interaction. It would be more powerful instead to attempt a non-local compensation of several interactions. For example, one could first split the ring into several blocks chosen by phase advance across the blocks. The beam-beam interactions within each block would be compensated by one of these multiple wire units. The non-linear map of each block of beam-beam interactions could then be minimized up to a certain order by appropriate choice of the wire parameters. We could also consider resonance compensation with these devices if that is a desirable strategy. For illustration, suppose we wish to compensate some 7th order resonances. Seventh order resonance driving terms in the Hamiltonian contributed by the beam-beam interactions and the wires can be written in the form

$$U_7 = Re \sum_p \sum_{m_x, m_y; m_x + m_y = 7} [U_{m_x, m_y, p}^{7, bb} + U_{m_x, m_y, p}^{7, wire}] e^{i(m_x \nu_x + m_y \nu_y - p)\theta} \quad (86)$$

The expressions for the beam-beam terms  $U_{m_x, m_y, p}^{7, bb}$  and the wire terms  $U_{m_x, m_y, p}^{7, wire}$  can be found in Appendix A and B respectively. If for example we wish to compensate the skew resonances  $7\nu_y = p$  and  $2\nu_x + 5\nu_y = p$ , we will require 4 wires to cancel the sine and cosine parts of these resonances and we will use the above equation to determine the skew coefficients  $a_6(1), \dots, a_6(4)$ . If a solution exists, then at a given radius this determines the azimuthal locations  $\phi_1, \dots, \phi_4$  of these wires. What advantage do these wires have over a conventional multipole magnet, say a 14-pole magnet to compensate 7th order resonances? The order of the resonances to be compensated could be changed by a different choice of the currents and angles  $\phi$ . This could be achieved by either having wires that could be moved along the circumference (technically hard) or by installing several wires and powering a selected few. In any event, multiple wires allow several strategies to be investigated.

## 6 Summary

Our purpose was to determine the feasibility of compensating the long-range interactions in the Tevatron with wires. The first case in chronological order that we studied was at injection energy where all the beam-beam interactions are long-range. In this theoretical study we placed a single wire in each of 4 warm straight sections. Using primarily a numerical optimization method, we found currents and positions for the 4 wires that increased the dynamic aperture of an anti-proton bunch by about  $2\sigma$ . Nearly the same increase was found with an independent code [5]. An alternative method of minimizing the norm of a nonlinear map found nearly the same values of the optimum wire parameters. These results indicated that wires could be useful. However it is not clear how either strategy could be implemented operationally.

At collision energy we focused first on locally correcting individual parasitics with the field of a single wire. The compensation works quite well when the strong beam is round so that the field profile of the strong bunch is well matched by the  $1/r$  field of a wire. But the obvious candidates that need compensation are the parasitics nearest the IPs where the beam separations are small and the beta functions large. The strong beam at these locations is very elliptical. None of the compensation strategies that were tried were successful because the field profile from the strong beam cannot be matched by a round wire. We developed analytical expressions for the field of a wire with an elliptical cross-section. Such wires were found to approximate the field of an elliptical beam quite well outside the core of the beam. These wires have not yet been tested in simulations. We next developed strategies for non-local compensation based on minimizing the phase space distortion. These helped us specify the ideal phase advances and the transverse positions of the compensating wire. The norm of the nonlinear map decreased by 25-35% at the best wire parameters. We tested these solutions on the 4 parasitics around B0 and D0. Unfortunately the diffusion, as calculated by numerical tracking, with the optimum wire settings did not decrease but increased.

We are led to conclude that successful compensation of the long-range interactions in the Tevatron cannot be achieved by single wires placed at a few locations. It is possible that strategies other than the ones we discussed may succeed - some we thought about but did not pursue. A successful strategy might involve multiple wires, perhaps with elliptical cross-sections, at several locations. Demonstrating that such a compensation works in a robust fashion will be challenging.

### Acknowledgements

We are indebted to H. Edwards, D. Finley, J.P. Koutchouk, J. Marriner and F. Zimmermann for reviewing the initial stages of this project in October 2003 and making several constructive suggestions. We also thank F. Zimmermann for joining our investigations in December 2003 and checking some of our results with his code. We thank P. Bhat, V. Shiltsev and M. Syphers for their support and patience during these studies.

## A Appendix: Optics changes due to beam-beam interactions

### Notation

$N_p$	Proton bunch intensity
$r_p$	classical proton radius
$\gamma_p$	Relativistic gamma
$N_{bb}$	Number of beam-beam interactions
$\sigma_x, \sigma_y$	rms beam sizes of protons
$D_x, D_y$	Physical separation between the centroids of protons and anti-protons
$x, y$	Coordinates of test anti-proton

### Orbit Shifts

The kicks on an anti-proton due to the proton beam can be found by numerical integration of

$$\begin{aligned}\Delta x' &= -\frac{N_p r_p}{\gamma_p} \frac{A_x}{\sigma_x} \int_0^1 \frac{dv}{[1+v(r^2-1)]^{1/2}} \exp[-\frac{1}{2}(A_x^2 + f A_y^2)v] \\ \Delta y' &= -\frac{N_p r_p}{\gamma_p} \frac{A_y}{\sigma_y} \int_0^1 \frac{dv}{[1+v(r^2-1)]^{1/2}} f \exp[-\frac{1}{2}(A_x^2 + f A_y^2)v]\end{aligned}\quad (\text{A.1})$$

$$f \equiv \frac{r^2}{1+v(r^2-1)}, \quad r = \frac{\sigma_y}{\sigma_x}, \quad A_x = \frac{x+D_x}{\sigma_x}, \quad A_y = \frac{y+D_y}{\sigma_y} \quad (\text{A.2})$$

The orbit shifts at any location  $s$  due to all the beam-beam interactions are

$$\Delta x_{bb}(s) = \frac{\sqrt{\beta_x(s)}}{2 \sin \pi \nu_x} \sum_{i=1}^{N_{bb}} \Delta x'_i \sqrt{\beta_{x,i}} \cos[|\psi_x(s) - \psi_{x,i}| - \pi \nu_x] \quad (\text{A.3})$$

$$\Delta y_{bb}(s) = \frac{\sqrt{\beta_y(s)}}{2 \sin \pi \nu_y} \sum_{i=1}^{N_{bb}} \Delta y'_i \sqrt{\beta_{y,i}} \cos[|\psi_y(s) - \psi_{y,i}| - \pi \nu_y] \quad (\text{A.4})$$

### Amplitude dependent tune shifts

The amplitude dependent tune shift in  $x$  is [7]

$$\Delta \nu_x(a_x, a_y, d_x, d_y, r) = \frac{4\pi C}{\varepsilon_x} \int_0^1 \frac{e^{-(p_x+p_y)}}{v[v(r^2-1)+1]^{1/2}} \sum_x \sum_y dv, \quad (\text{A.5})$$

where

$$\sum_x = \sum_{k=0}^{\infty} \frac{\left(\frac{a_x}{d_x}\right)^k}{k!} \Gamma\left(k + \frac{1}{2}\right) \left[ I_k(s_x) \left( \frac{2k}{a_x^2} - v \right) + I_{k+1}(s_x) \frac{s_x}{a_x^2} \right], \quad (\text{A.6})$$

$$\sum_y = \sum_{l=0}^{\infty} \frac{\left(\frac{a_y}{d_y}\right)^l}{l!} \Gamma\left(l + \frac{1}{2}\right) I_l(s_y). \quad (\text{A.7})$$

$I_m$  are the modified Bessel functions. There are similar expressions for the amplitude dependent tune shift in  $y$  [7].

For round beams these can be simplified. If the beta functions on the proton and anti-proton helices are nearly the same and the proton momentum spread  $\delta_p$  is negligibly small or there is no dispersion  $\eta_{x,p} = 0, \eta_{y,p} = 0$ , then writing the dimensionless separations  $d_x, d_y$  as

$$d_x = d \cos \theta, \quad d_y = d \sin \theta$$

the small amplitude tune shifts for round beams are

$$\Delta\nu_x = \frac{N_p r_p}{4\pi\epsilon_{x,p}^N} \frac{2}{d^2} [\cos 2\theta + (d^2 \cos^2 \theta + \cos 2\theta) \exp(-\frac{1}{2}d^2)] \quad (\text{A.8})$$

$$\Delta\nu_y = \frac{N_p r_p}{4\pi\epsilon_{y,p}^N} \frac{2}{d^2} [-\cos 2\theta + (d^2 \sin^2 \theta - \cos 2\theta) \exp(-\frac{1}{2}d^2)] \quad (\text{A.9})$$

At large separations  $d \gg 1$ , these further simplify to

$$\Delta\nu_x = \frac{N_p r_p}{4\pi\epsilon_p^N} \frac{2}{d^2} \cos 2\theta = -\Delta\nu_y \quad (\text{A.10})$$

### Resonance driving terms

The potential  $U_{bb}$  due to the beam-beam interactions can be written in terms of the resonance driving terms  $U_{m_x, m_y, p}^{bb}$  as

$$U_{bb} = \mathbf{Re} \left[ \sum_p \sum_{m_x} \sum_{m_y} U_{m_x, m_y, p}^{bb} \exp[i(m_x \nu_x + m_y \nu_y - p)\theta] \right] \quad (\text{A.11})$$

The resonance driving terms are evaluated by summing over the  $N_{bb}$  interactions,

$$\begin{aligned} U_{m_x, m_y, p}^{bb} &= (-1)^{m_x + m_y + 1} \frac{r_p}{2\pi\gamma_p} \sum_j^{N_{bb}} N_{p,j} \int_0^1 \frac{dv}{v[v(r^2 - 1) + 1]^{1/2}} \exp(-t_{x,j} - t_{y,j}) X_j Y_j \\ &\quad \times \exp[i(m_x \psi_{x,j} + m_y \psi_{y,j} + p\theta_j)] \end{aligned} \quad (\text{A.12})$$

where

$$\begin{aligned} X_j &= \sum_{l=-\infty}^{\infty} (-1)^l \exp(-r_{x,j}) I_{m_x+2l}(r_{x,j}) \exp(-s_{x,j}) I_l(s_{x,j}) \\ Y_j &= \sum_{l=-\infty}^{\infty} (-1)^l \exp(-r_{y,j}) I_{m_y+j+2l}(r_{y,j}) \exp(-s_{y,j}) I_l(s_{y,j}) \\ r_{x,j} &= a_{x,j} d_{x,j} v, \quad s_{x,j} = \frac{1}{4} a_{x,j}^2 v, \quad t_{x,j} = \frac{1}{2} d_{x,j} (d_{x,j} - 2a_{x,j}) v \\ r_{y,j} &= f a_{y,j} d_{y,j} v, \quad s_{y,j} = \frac{1}{4} f a_{y,j}^2 v, \quad t_{y,j} = \frac{1}{2} f d_{y,j} (d_{y,j} - 2a_{y,j}) v \\ a_{x,j} &= \frac{\sqrt{2\beta_{x,j} J_x}}{\sigma_{x,j}}, \quad a_{y,j} = \frac{\sqrt{2\beta_{y,j} J_y}}{\sigma_{y,j}} \end{aligned}$$

$J_x, J_y$  are the linear actions at the amplitude of interest.

## B Appendix: Optics changes due to the field of a wire

### Notation

$N_p$	Proton bunch intensity
$r_p$	classical proton radius
$\gamma_p$	Relativistic gamma
$N_{bb}$	Number of beam-beam interactions
$\sigma_x, \sigma_y$	rms beam sizes of protons
$D_x, D_y$	Physical separation between the centroids of protons and anti-protons
$x, y$	Coordinates of test anti-proton
$r_W$	radial distance from the origin to the wire
$\phi_W$	angle of the wire position with the positive $x$ axis
$(x, y)$	coordinates of the anti-proton
$I, L$	current and length of wire

### Wire kicks

The kicks due to an infinitely long wire with a round cross-section are

$$\Delta x' = \frac{\mu_0}{2\pi} \frac{IL}{(B\rho)} \frac{r_W \cos \phi_W - x}{r_W^2 + x^2 + y^2 - 2r_W(x \cos \phi_W + y \sin \phi_W)} \quad (\text{B.1})$$

$$\Delta y' = \frac{\mu_0}{2\pi} \frac{IL}{(B\rho)} \frac{r_W \sin \phi_W - y}{r_W^2 + x^2 + y^2 - 2r_W(x \cos \phi_W + y \sin \phi_W)} \quad (\text{B.2})$$

### Closed Orbit Shifts

The closed orbit shifts at any location  $s$  are

$$\Delta x_W(s) = \frac{\sqrt{\beta_x(s)}}{2 \sin \pi \nu_x} \Delta x' \sqrt{\beta_x} \cos[|\psi_x(s) - \psi_x| - \pi \nu_x] \quad (\text{B.3})$$

$$\Delta y_W(s) = \frac{\sqrt{\beta_y(s)}}{2 \sin \pi \nu_y} \Delta y' \sqrt{\beta_y} \cos[|\psi_y(s) - \psi_y| - \pi \nu_y] \quad (\text{B.4})$$

### Tune shifts at zero amplitude

$$\Delta \nu_x = -\frac{\mu_0}{8\pi^2(B\rho)} \beta_x \left[ \frac{I_W L \cos 2\theta_W}{r_W^2} \right], \quad \Delta \nu_y = +\frac{\mu_0}{8\pi^2(B\rho)} \beta_y \left[ \frac{I_W L \cos 2\theta_W}{r_W^2} \right]$$

Both tune shifts have the same dependence on the wire parameters in square brackets [ ].

### Minimum tune split

The wire also introduces coupling characterized by the minimum tune split between the transverse planes

$$\Delta \nu_{min} = \frac{\mu_0}{4\pi^2(B\rho)} \sqrt{\beta_x \beta_y} \left[ \frac{I_W L \sin 2\theta_W}{r_W^2} \right]$$

The minimum tune split is of the same order as the tune shift.

The eigen tunes are

$$\nu_{\pm} = \frac{1}{2}(\nu_x + \nu_y) \pm \frac{1}{2}\Delta, \quad \Delta = [(\nu_x - \nu_y)^2 + \Delta \nu_{min}^2]^{1/2} \quad (\text{B.5})$$

## Zero amplitude chromaticities

$$\begin{aligned}\nu'_x &= \frac{\mu_0}{4\pi^2} \frac{I_W L}{(B\rho)} \frac{\beta_x}{r_W^3} [D_x \cos 3\theta_W + D_y \sin 3\theta_W] \\ \nu'_y &= -\frac{\mu_0}{4\pi^2} \frac{I_W L}{(B\rho)} \frac{\beta_y}{r_W^3} [D_x \cos 3\theta_W + D_y \sin 3\theta_W]\end{aligned}\quad (\text{B.6})$$

## Tune spread

The scalar potential due to the wire that contributes to the Hamiltonian is

$$U = -\frac{\mu_0}{2\pi} \frac{IR}{(B\rho)} \ln r \quad (\text{B.7})$$

where  $R = C/(2\pi)$  is the average radius of the ring. From the expression for the tune shift

$$\Delta\nu_x = \frac{1}{2\pi} \int \int \frac{d\phi_x}{2\pi} \frac{d\phi_y}{2\pi} \frac{\partial}{\partial J_x} U \quad (\text{B.8})$$

and a similar expression for  $\Delta\nu_y$ , it follows that

$$\Delta\nu_x = -\left(\frac{\mu_0 IL}{4\pi^2(B\rho)}\right) \int \int \frac{d\phi_x}{2\pi} \frac{d\phi_y}{2\pi} \frac{\beta_x \cos^2 \phi_x - r_W \sqrt{\beta_x/(2J_x)} \cos \phi_x \cos \phi_W}{A + B_x \cos \phi_x + B_y \cos \phi_y + C_x \cos^2 \phi_x + C_y \cos^2 \phi_y} \quad (\text{B.9})$$

$$\Delta\nu_y = -\left(\frac{\mu_0 IL}{4\pi^2(B\rho)}\right) \int \int \frac{d\phi_x}{2\pi} \frac{d\phi_y}{2\pi} \frac{\beta_y \cos^2 \phi_y - r_W \sqrt{\beta_y/(2J_y)} \cos \phi_y \sin \phi_W}{A + B_x \cos \phi_x + B_y \cos \phi_y + C_x \cos^2 \phi_x + C_y \cos^2 \phi_y} \quad (\text{B.10})$$

where

$$A = r_W^2, \quad B_x = -2\sqrt{2}r_W \sqrt{\beta_x J_x} \cos \phi_W, \quad B_y = -2\sqrt{2}r_W \sqrt{\beta_y J_y} \sin \phi_W \quad (\text{B.11})$$

$$C_x = 2\beta_x J_x, \quad C_y = 2\beta_y J_y \quad (\text{B.12})$$

## Resonance driving terms

The potential due to the wire using the multipole expansion can be written as

$$\begin{aligned}U &= B_{0,W} R \operatorname{Re} \left[ \sum_p \sum_m \sum_{m_x=-m}^m \sum_{m_y=-n+1-m}^{n+1-m} J_x^{m/2} J_y^{(n+1-m)/2} [\tilde{B}_{nm;m_x,m_y;p} + \tilde{A}_{nm;m_x,m_y;p}] \right. \\ &\quad \times \exp[i(m_x \nu_x + m_y \nu_y - p)\theta] \left. \right] \quad (\text{B.13})\end{aligned}$$

where

$$\begin{aligned}\sum_m \tilde{B}_{nm;m_x,m_y;p} &= \sum_{m=0(n \text{ odd}), 1(n \text{ even}); \Delta m=2}^{n+1} \tilde{B}_{nm;m_x,m_y;p} \\ \sum_m \tilde{A}_{nm;m_x,m_y;p} &= \sum_{m=0(n \text{ even}), 1(n \text{ odd}); \Delta m=2}^n \tilde{A}_{nm;m_x,m_y;p}\end{aligned}$$

In the sums over  $(m_x, m_y)$ , these integers also advance by 2 over successive terms. e.g.  $m_x = -m, -m + 2, -m + 4, \dots, m - 2, m$  etc.

The Fourier coefficients are

$$\tilde{B}_{nm;m_x,m_y;p} = \frac{1}{2\pi} \int_0^{2\pi} B_{nm;m_x,m_y}(\theta) e^{ip\theta} d\theta, \quad \tilde{A}_{nm;m_x,m_y;p} = \frac{1}{2\pi} \int_0^{2\pi} A_{nm;m_x,m_y}(\theta) e^{ip\theta} d\theta \quad (\text{B.15})$$

and

$$B_{nm; m_x, m_y} = \frac{(-1)^{(n+1-m)/2} b_n}{(n+1)2^{(n+1)/2}} \beta_x^{m/2} \beta_y^{(n+1-m)/2} \left( \begin{array}{c} n+1 \\ m \end{array} \right) \left( \begin{array}{c} m \\ (m+m_x)/2 \end{array} \right) \left( \begin{array}{c} n+1-m \\ (n+1-m+m_y)/2 \end{array} \right) \times \exp[i(m_x \psi_x(\theta) + m_y \psi_y(\theta))] \quad (\text{B.16})$$

$$A_{nm; m_x, m_y} = \frac{(-1)^{(n+2-m)/2} a_n}{(n+1)2^{(n+1)/2}} \beta_x^{m/2} \beta_y^{(n+1-m)/2} \left( \begin{array}{c} n+1 \\ m \end{array} \right) \left( \begin{array}{c} m \\ (m+m_x)/2 \end{array} \right) \left( \begin{array}{c} n+1-m \\ (n+1-m+m_y)/2 \end{array} \right) \times \exp[i(m_x \psi_x(\theta) + m_y \psi_y(\theta))] \quad (\text{B.17})$$

where  $\psi_x, \psi_y$  are the periodic parts of the betatron phase,

$$\psi_x(\theta + 2\pi) = \psi_x, \quad \psi_y(\theta + 2\pi) = \psi_y$$

Each  $n$ th order resonances  $[|m_x| + |m_y| = n]$  is driven by the coefficients  $(b_{n-1}, a_{n-1})$  but also the coefficients  $(b_{n+1}, a_{n+1}), (b_{n+3}, a_{n+3}), \dots$ . The  $n$ th order resonances are known as the *sub-resonance* of the higher order coefficients.

## C Appendix: Average beam-beam kick

Here we derive the expression of the average beam-beam kick. Assume that both beams (strong and weak) are Gaussian beams, but not round. Denote the rms beam sizes by  $(\sigma_x, \sigma_y)$  for the strong beam and  $(\bar{\sigma}_x, \bar{\sigma}_y)$  for the weak beam. The kick felt by a particle in the weak beam with betatron amplitudes  $(x, y)$  is given by

$$\Delta x' = -\frac{2N_b r_p (x_p - x)}{\gamma_p} \int_0^\infty \frac{dq}{(2\sigma_x^2 + q)^{3/2} (2\sigma_y^2 + q)^{1/2}} \times \quad (\text{C.1})$$

$$\exp \left( -\frac{(x_p - x)^2}{2\sigma_x^2 + q} - \frac{(y_p - y)^2}{2\sigma_y^2 + q} \right),$$

$$\Delta y' = -\frac{2N_b r_p (y_p - y)}{\gamma_p} \int_0^\infty \frac{dq}{(2\sigma_x^2 + q)^{1/2} (2\sigma_y^2 + q)^{3/2}} \times \quad (\text{C.2})$$

$$\exp \left( -\frac{(x_p - x)^2}{2\sigma_x^2 + q} - \frac{(y_p - y)^2}{2\sigma_y^2 + q} \right),$$

where  $(x_p, y_p)$  denotes the location of the strong beam centroid w.r.t. the closed orbit of the weak beam.

The density distribution function of the weak beam is given by

$$\rho(x, y) = \frac{1}{2\pi\bar{\sigma}_x\bar{\sigma}_y} \exp \left( -\frac{x^2}{2\bar{\sigma}_x^2} - \frac{y^2}{2\bar{\sigma}_y^2} \right). \quad (\text{C.3})$$

Therefore, the average kick given to the weak beam is obtained as

$$\langle \Delta x' \rangle = \int_{-\infty}^\infty dx \int_{-\infty}^\infty dy \Delta x' \rho(x, y), \quad \langle \Delta y' \rangle = \int_{-\infty}^\infty dx \int_{-\infty}^\infty dy \Delta y' \rho(x, y). \quad (\text{C.4})$$

Due to the smoothness of the integrand we can change the order of the integration, and write the relations as

$$\langle \Delta x' \rangle = -\frac{2N_b r_p}{\gamma_p} \frac{1}{2\pi\bar{\sigma}_x\bar{\sigma}_y} \int_0^\infty \frac{dq}{(2\sigma_x^2 + q)^{3/2} (2\sigma_y^2 + q)^{1/2}} I_x(q) I_y(q), \quad (\text{C.5})$$

where

$$I_x(q) = \int_{-\infty}^\infty dx (x_p - x) \exp \left( -\frac{(x_p - x)^2}{2\sigma_x^2 + q} - \frac{x^2}{2\bar{\sigma}_x^2} \right), \quad (\text{C.6})$$

$$I_y(q) = \int_{-\infty}^\infty dy \exp \left( -\frac{(y_p - y)^2}{2\sigma_y^2 + q} - \frac{y^2}{2\bar{\sigma}_y^2} \right). \quad (\text{C.7})$$

The integrations can be done analytically, and give the following results:

$$I_x(q) = \frac{\sqrt{2\pi}\bar{\sigma}_x (2\sigma_x^2 + q)^{3/2} x_p}{[2(\sigma_x^2 + \bar{\sigma}_x^2) + q]^{3/2}} \exp \left[ -\frac{x_p^2}{2(\sigma_x^2 + \bar{\sigma}_x^2) + q} \right], \quad (\text{C.8})$$

$$I_y(q) = \frac{\sqrt{2\pi}\bar{\sigma}_y (2\sigma_y^2 + q)^{1/2}}{[2(\sigma_y^2 + \bar{\sigma}_y^2) + q]^{1/2}} \exp \left[ -\frac{y_p^2}{2(\sigma_y^2 + \bar{\sigma}_y^2) + q} \right]. \quad (\text{C.9})$$

Hence

$$\begin{aligned} \langle \Delta x' \rangle &= -\frac{2N_b r_p x_p}{\gamma_p} \int_0^\infty \frac{dq}{[2(\sigma_x^2 + \bar{\sigma}_x^2) + q]^{3/2} [2(\sigma_y^2 + \bar{\sigma}_y^2) + q]^{1/2}} \times \\ &\quad \exp \left[ -\frac{x_p^2}{2(\sigma_x^2 + \bar{\sigma}_x^2) + q} - \frac{y_p^2}{2(\sigma_y^2 + \bar{\sigma}_y^2) + q} \right], \end{aligned} \quad (\text{C.10})$$

that is,  $\langle \Delta x' \rangle$  is the kick felt by the weak beam's centroid from a beam with an effective beam size being equal with the rms beam size of the strong and weak beams. Due to symmetry in  $x$  and  $y$ ,  $\langle \Delta y' \rangle$  looks similar, i.e.  $\langle \Delta x' \rangle$  with  $x$  and  $y$  interchanged. Of course, the numerical evaluation of the average kick is done more efficiently utilizing the well-known Bassetti-Erskine formulae.

### C.1 Special case of round beams

To check the result, the special case of round beams can be studied, where all integrals can be performed analytically. The single particle kick in this case is given by ( $\sigma = \sigma_x = \sigma_y$ )

$$\Delta x' = -\frac{2N_b r_p}{\gamma_p} \frac{x_p - x}{(x_p - x)^2 + (y_p - y)^2} \left[ 1 - \exp \left( -\frac{(x_p - x)^2 + (y_p - y)^2}{2\sigma^2} \right) \right], \quad (\text{C.11})$$

$$\Delta y' = -\frac{2N_b r_p}{\gamma_p} \frac{y_p - y}{(x_p - x)^2 + (y_p - y)^2} \left[ 1 - \exp \left( -\frac{(x_p - x)^2 + (y_p - y)^2}{2\sigma^2} \right) \right]. \quad (\text{C.12})$$

The integrals in this case cannot be separated into integrations over  $x$  and  $y$  independently, so we switch to polar coordinates using

$$x_p - x = r \cos \phi, \quad (\text{C.13})$$

$$y_p - y = r \sin \phi. \quad (\text{C.14})$$

The average kick becomes ( $\bar{\sigma} = \bar{\sigma}_x = \bar{\sigma}_y$ )

$$\langle \Delta x' \rangle = -\frac{2N_b r_p}{\gamma_p} \frac{1}{2\pi\bar{\sigma}^2} \exp \left( -\frac{x_p^2 + y_p^2}{2\bar{\sigma}^2} \right) \int_0^\infty dr \left[ 1 - \exp \left( -\frac{r^2}{2\sigma^2} \right) \right] \exp \left( -\frac{r^2}{2\bar{\sigma}^2} \right) \quad (\text{C.15})$$

$$\times \int_0^{2\pi} d\phi \exp \left[ \frac{r(x_p \cos \phi + y_p \sin \phi)}{\bar{\sigma}^2} \right] \cos \phi. \quad (\text{C.16})$$

The integration over  $\phi$  is given by (from Integrals & Series, vol.1, page 464)

$$\int_0^{2\pi} d\phi \exp \left[ \frac{r(x_p \cos \phi + y_p \sin \phi)}{\bar{\sigma}^2} \right] \cos \phi = \frac{2\pi x_p}{\sqrt{x_p^2 + y_p^2}} I_1 \left( \frac{r\sqrt{x_p^2 + y_p^2}}{\bar{\sigma}^2} \right), \quad (\text{C.17})$$

where  $I_1(z)$  is the modified Bessel function. If we denote by  $d = \sqrt{x_p^2 + y_p^2}$ , the last integral to be done is

$$\int_0^\infty dr \left[ 1 - \exp \left( -\frac{r^2}{2\sigma^2} \right) \right] \exp \left( -\frac{r^2}{2\bar{\sigma}^2} \right) I_1 \left( \frac{d}{\bar{\sigma}^2} r \right). \quad (\text{C.18})$$

Mathematica gives the result

$$\frac{\bar{\sigma}^2}{d} \left\{ \exp \left( \frac{d^2}{2\bar{\sigma}^2} \right) - \exp \left[ \frac{d^2 \sigma^2}{2\bar{\sigma}^2 (\sigma^2 + \bar{\sigma}^2)} \right] \right\}. \quad (\text{C.19})$$

Combining everything we recover the special case result

$$\langle \Delta x' \rangle = -\frac{2N_b r_p}{\gamma_p} \frac{x_p}{d^2} \left\{ 1 - \exp \left[ -\frac{d^2}{2(\sigma^2 + \bar{\sigma}^2)} \right] \right\}, \quad (\text{C.20})$$

and analogously for  $\langle \Delta y' \rangle$ .

## References

- [1] J.P. Koutchouk, *Principle of a correction of the long-range beam-beam effect in LHC using electro-magnetic lenses*, LHC Project Note 223 (2000)
- [2] F. Zimmermann, *Weak-strong simulation studies for the LHC long-range beam-beam compensation*, Proc. of FNAL Workshop, Fermilab-Conf-01-390 (2001)
- [3] J.P. Koutchouk, J. Wenninger and F. Zimmermann, *Experiments on LHC long-range beam-beam compensation in the SPS*, EPAC 2004
- [4] Review of wire compensation October 2003,  
[http://www-bd.fnal.gov/run2upgrade/reviews/Tev\\_wire\\_BBC\\_Oct03.html](http://www-bd.fnal.gov/run2upgrade/reviews/Tev_wire_BBC_Oct03.html)
- [5] F. Zimmermann, T. Sen, B. Erdelyi and V. Boocha, *Study of long-range collisions and wire compensation for Tevatron Run II*, Beams-doc-1111 (2004)
- [6] BBSIM, beam-beam simulation code developed at FNAL by T. Sen, V. Boocha and B. Erdelyi,  
<http://waldo.fnal.gov/~tsen/BBCODE/public/>
- [7] T. Sen, B. Erdelyi, M. Xiao, V. Boocha, *Beam-beam effects in the Tevatron*, PRSTAB, Vol 7, 041001(2004)
- [8] COSY web site: [http://www.bt.pa.msu.edu/index\\_files/cosy.htm](http://www.bt.pa.msu.edu/index_files/cosy.htm)
- [9] Sixtrack web site: <http://frs.home.cern.ch/frs/>